Investigating aerosol–cloud interactions

Benjamin Stephen Grandey

Supervisor: Dr Philip Stier

Second year report
August 2010

Atmospheric, Oceanic and Planetary Physics
Department of Physics
University of Oxford

Word count: ∼14000 words

Investigating aerosol–cloud interactions

Abstract

Microphysical and dynamical interactions between clouds and aerosols are associated with some of the largest uncertainties in projections of future climate. Many possible aerosol effects on clouds have been suggested, but much more research is needed in order to estimate the size of these effects globally. In order to improve model projections of future climate, it is essential that we improve our quantitative understanding of these effects. Several studies investigating interactions between observed cloud and aerosol properties have been published in recent years. However, the observed correlations are not necessarily due to microphysical effects. They may be due to cloud flagging errors, retrieval errors, seasonal factors, spatial climatological factors, humidity conditions or synoptic effects.

This report presents a discussion of the contribution of spatial climatological and synoptic effects to aerosol–cloud relationships. Analysing satellite datasets over large regions may introduce spurious relationships between aerosol and cloud properties due to spatial variations in aerosol type, cloud regime and synoptic regime climatologies. Using MODerate resolution Imaging Spectroradiometer (MODIS) data, relationships between aerosol optical depth τ_a, derived liquid cloud droplet effective number concentration N_e and liquid cloud droplet effective radius r_e are calculated at different spatial scales. For region sizes larger than $4^\circ \times 4^\circ$, spurious spatial variations in retrieved cloud and aerosol properties are found to introduce widespread significant errors to calculations of $\frac{\mathrm{d}\ln N_e}{\mathrm{d}\ln \tau_a}$ and $\frac{\mathrm{d}\ln r_e}{\mathrm{d}\ln \tau_a}$. In order to assess the contribution of synoptic effects to observed aerosol–cloud relationships, discussion of a storm-centric methodology for analysing satellite retrieved aerosol and cloud data is also presented.

Contents

Chapter 1

Introduction

1.1 Aerosols, clouds and climate

1.1.1 What are atmospheric aerosols?

The Intergovernmental Panel on Climate Change (IPCC) defines *aerosols* as "airborne solid or liquid particles, with a typical size between 0.01 and 10 μm that reside in the atmosphere for at least several hours" [Forster et al., 2007]. The Earth's atmosphere contains many different kinds of aerosols, of both anthropogenic and natural origin. Some categories of aerosol which are considered to play an important role with regard to climate are sulphate, organic carbon, black carbon, nitrate, mineral dust and sea-salt aerosols [e.g., Haywood and Boucher, 2000].

1.1.2 Direct and indirect aerosol effects on climate

The optical and microphysical properties of aerosols may give rise to several radiative effects in the Earth's atmosphere. Figure 1.1 contains a schematic illustrating some of these potential effects.

The *direct aerosol effect* refers to scattering and absorption of shortwave and longwave radiation by atmospheric aerosols. The direct effect radiative perturbation due to a given aerosol is dependent on the vertical distribution of the aerosol, the *albedo* (reflectivity) of the Earth's surface beneath and any clouds present [e.g. Haywood and Shine, 1995, Stier et al., 2007]. For example, for aerosols over a surface with a high albedo, such as snow or cloud, any absorption by the aerosol may dominate over scattering effects, leading to a net warming effect.

Heating due to the absorption of shortwave radiation by tropospheric aerosols can lead to increased temperatures in the aerosol layer, decreasing relative humidity and changing tropospheric stability. This can significantly affect cloud lifetime, and is known as the *semi-direct aerosol effect*. For example, a modelling study showed that absorption of shortwave radiation by black carbon aerosol can lead to an enhanced daytime clearing of trade cumulus clouds over the northern Indian Ocean [Ackerman et al., 2000].

Indirect aerosol effects are the radiative effects which aerosols can have through microphysical interactions with clouds. Many aerosols are effective cloud condensation nuclei. A strong correlation between cloud condensation nuclei concentrations and aerosol optical depth has been observed [Andreae, 2009]. Increasing the aerosol concentration in a cloud can lead to increased numbers of cloud condensation nuclei competing for water vapour which, in a cloud of constant liquid water content, in turn leads to a greater number of smaller droplets. This increases the albedo of the cloud [Twomey, 1977], resulting in more shortwave radiation being reflected to space, and is referred to as the *cloud albedo effect*. Precipitation can be suppressed and the lifetime of the cloud can be affected [Albrecht, 1989], an effect known as the *cloud lifetime effect*. The cloud top height can also be affected [Pincus and Baker, 1994]. Other indirect effects have been suggested, such as the *glaciation indirect effect*,

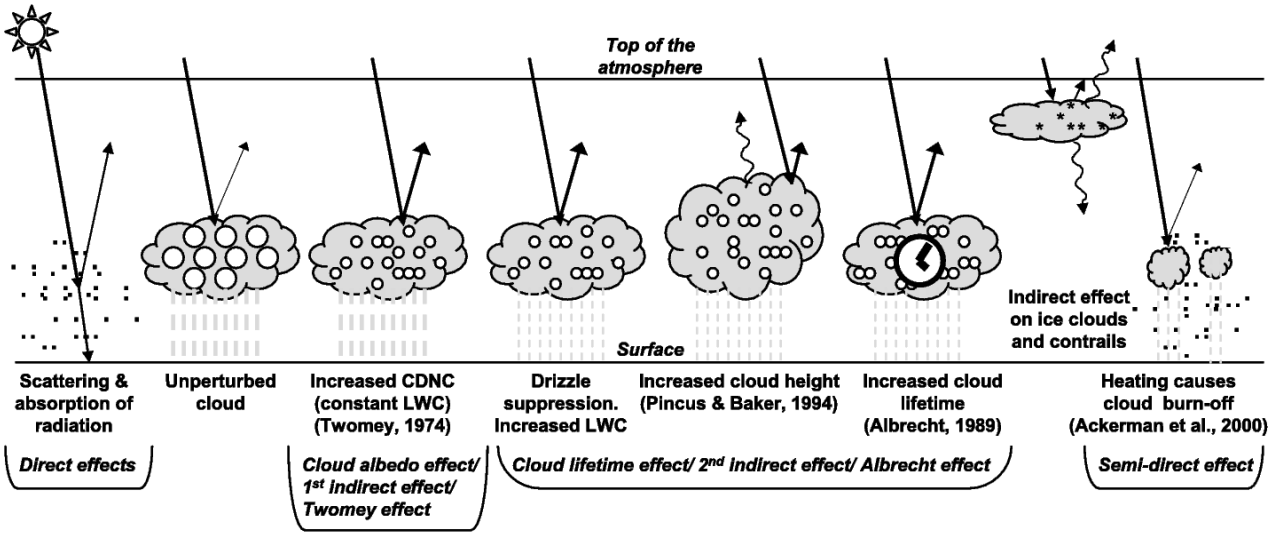

Figure 1.1: Schematic diagram showing the various radiative mechanisms associated with cloud effects that have been identified in relation to aerosols. The small black dots represent aerosol particles, the larger open circles cloud droplets. Straight lines represent the incident and reflected solar radiation, and wavy lines represent terrestrial radiation. The filled white circles indicate cloud droplet number concentration. The unperturbed cloud contains larger cloud drops because only natural aerosols are available as cloud condensation nuclei, while the perturbed cloud contains a greater number of smaller cloud drops because both natural and anthropogenic aerosols are available as cloud condensation nuclei. The vertical grey dashes represent rainfall, and LWC refers to liquid water content. [Figure taken from Forster et al., 2007.]

proposed by Lohmann [2002], whereby black carbon aerosols act as effective ice nuclei and can therefore enhance precipitation in the ice phase.

A complex interplay between different aerosol effects and feedbacks may exist in any given real-world situation. For example, Koren et al. [2008] propose that for clouds in smoky conditions over the Amazon, microphysical (indirect) aerosol effects dominate for low aerosol conditions and radiative (semi-direct) aerosol effects on the clouds dominate in high aerosol conditions.

It is worth noting that most aerosols have a much shorter lifetime than greenhouse gases, and so have a much stronger regional distribution and remain in the atmosphere for a much shorter period of time. Since many aerosol species can lead to health problems [see e.g. Bell et al., 2004, Kennedy, 2007], increasingly cleaner technologies are being employed in order to decrease aerosol emissions. Indeed, European emissions of sulphur have decreased by 70 % since 1980 [Grennfelt and Hov, 2005]. As a result, due to their short lifetime, the atmospheric concentration of aerosols is unlikely to increase significantly. Under these conditions, future warming due to the increasing greenhouse gas concentrations will increasingly dominate over aerosol radiative effects [Andreae et al., 2005, Kiehl, 2007]. Uncertainties in the size of aerosol radiative effects lead to uncertainties in the sensitivity of the climate's response to greenhouse gas forcing. In order to accurately forecast future warming trends, it is therefore important to quantify the significance of aerosol effects in the present, and to reduce the large uncertainty in the radiative forcing due to aerosols.

1.1.3 Radiative forcing, climate feedbacks and projection uncertainties

Radiative forcing is "the change in the net, downward minus upward, irradiance (expressed in Wm^{-2}) at the tropopause due to a change in an external driver of climate change" [Forster et al., 2007]. Positive radiative forcings lead to a warming of the climate system. Significant forcings regularly considered in attribution studies are those caused by changes in the solar constant, greenhouse gas

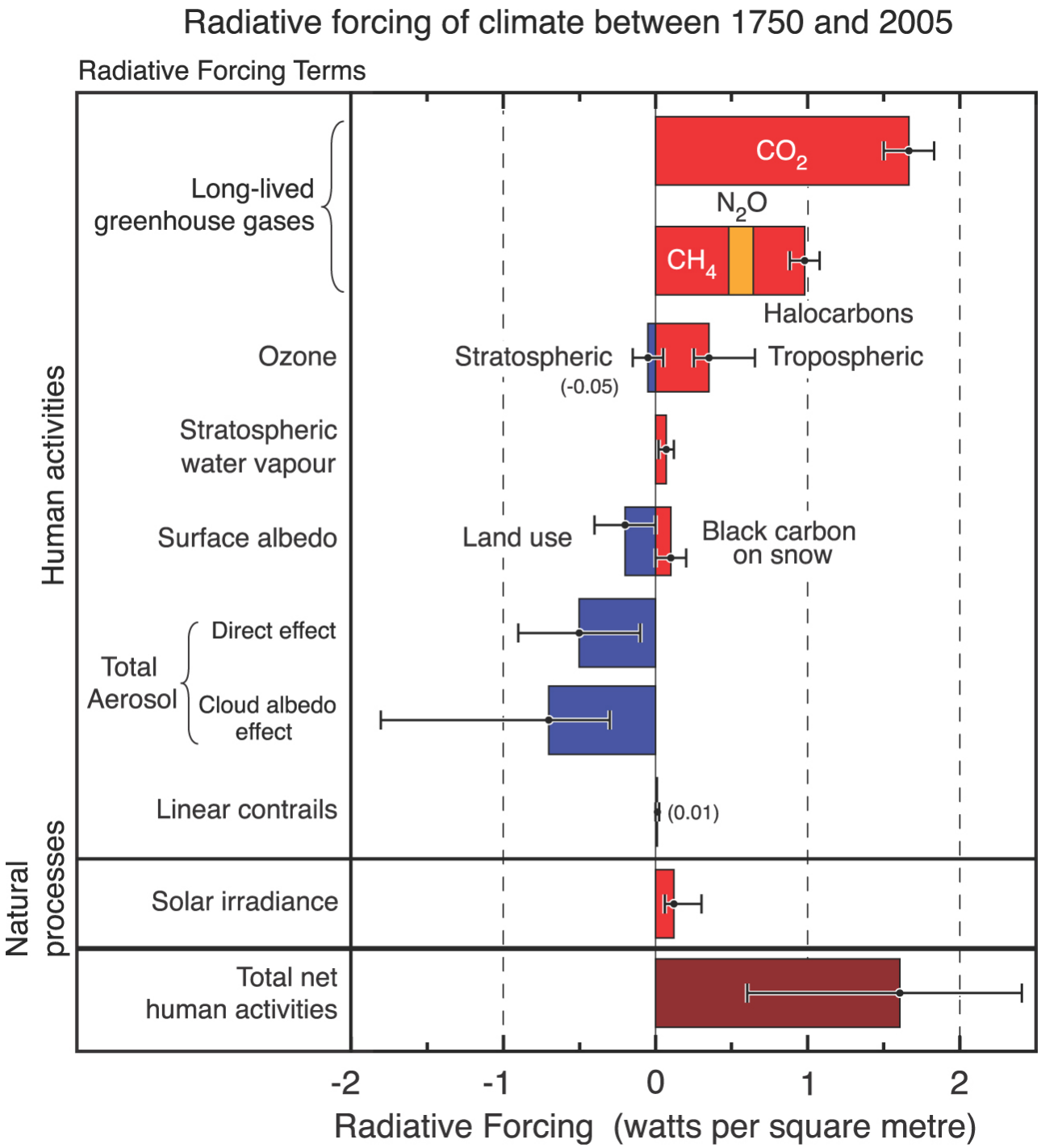

Figure 1.2: Summary of the principal components of the radiative forcing of climate change. The values represent the forcings in 2005 relative to the start of the industrial era (about 1750). Human activities cause significant changes in long-lived gases, ozone, water vapour, surface albedo, aerosols and contrails. The only increase in natural forcing of any significance between 1750 and 2005 occurred in solar irradiance. The thin black line attached to each coloured bar represents the range of uncertainty for the respective value. [Figure taken from Forster et al., 2007.]

concentrations, tropospheric sulphate aerosols and stratospheric volcanic aerosols [e.g. Stone et al., 2007]. Figure 1.2 summarises the climatic radiative forcing components identified by Forster et al. [2007].

Many mechanisms act either to intensify or to oppose changes in the climate system. These effects

are known as *climate feedbacks*. For example, if a surface-air temperature increase in polar regions reduces snow cover, the surface albedo will be reduced and less solar radiation will be reflected, creating a positive feedback mechanism leading to a greater warming in these regions. Several major climate feedbacks are those associated with clouds, water vapour, the lapse rate and the cryosphere [Bony et al., 2006].

As shown in Figure 1.2, Forster et al. [2007] estimate an aerosol direct effect radiative forcing of -0.5 [-0.9 to -0.1] Wm^{-2} and a cloud albedo effect of -0.7 [-1.8 to -0.3] Wm^{-2}. Due to their interaction with the hydrological cycle, the other indirect effects and semi-direct effect are not considered as radiative forcings by Forster et al. [2007]. However, Lohmann and Feichter [2005] estimate an effective cloud lifetime effect radiative forcing of -1.2 [-1.9 to -0.5] Wm^{-2}, leading to a total net anthropogenic radiative forcing of 0.4 [-0.3 to 2.4] Wm^{-2}. As can be seen, there is a large uncertainty in the present-day total anthropogenic radiative forcing, and most of this uncertainty is due to uncertainties in the size of aerosol effects.

1.2 Observational tools

Observations play an integral role in helping us to improve our understanding of the highly complex processes which occur in the atmosphere. They often highlight new avenues for investigation. They form the basis for scientific hypotheses. And they act as the plumbline by which theories must be assessed. As the physicist Richard Feynman famously said, "if it disagrees with experiment it is wrong" [Feynman, 2007]. This applies as much to atmospheric science as it does to fundamental physics. Observations help scientific research to remain rooted in reality.

Many observational datasets of the atmosphere exist. Some are produced using in situ surface, ship and aircraft measurments, such as those gathered during the Variability of the American Monsoon System (VAMOS) Ocean–Cloud–Atmosphere–Land Study Regional Experiment (VOCALS-REx) field campaign [Wood et al., 2007]. Other datasets contain data that has been remotely sensed from the surface, such as the aerosol data retrieved from the AErosol RObotic NETwork (AERONET) [Holben et al., 1998]. However, the observational datasets most widely used for aerosol–cloud interaction studies are those retrieved from satellite data.

1.2.1 Satellite platforms

Terra

Terra, also known as Earth Observing System (EOS) AM-1, was launched on 18$^{\text{th}}$ December 1999 and acts as a platform for a number of instruments: ASTER (Advanced Spaceborne Thermal Emission and Reflection Radiometer), CERES (Clouds and Earth's Radiant Energy System), MISR (Multiangle Imaging SpectroRadiometer), MODIS (MODerate resolution Imaging Spectroradiometer) and MOPITT (Measurements Of Pollution In The Troposphere) [NASA, 2009b]. It is in a sun-synchronous orbit with a 10:30 A.M. equatorial crossing time [Kaufman et al., 1998].

Envisat

Envisat, launched in March 2002, is in a sun-synchronous orbit with a southwards equatorial crossing time of 10:00 A.M. [ESA, 2009]. It carries ASAR (Advanced Synthetic Aperture Radar), MERIS (Medium Resolution Imaging Spectrometer), AATSR (Advanced-Along Track Scanning Radiometer), RA-2 (Radar Altimeter 2), GOMOS (a medium resolution spectrometer), MIPAS (Michelson Interferometer for Passive Atmospheric Sounding), SCIAMACHY (an imaging spectrometer), DORIS (Doppler Orbitography and Radio-positioning Integrated by Satellite) and LRR (Laser Retro-Reflector).

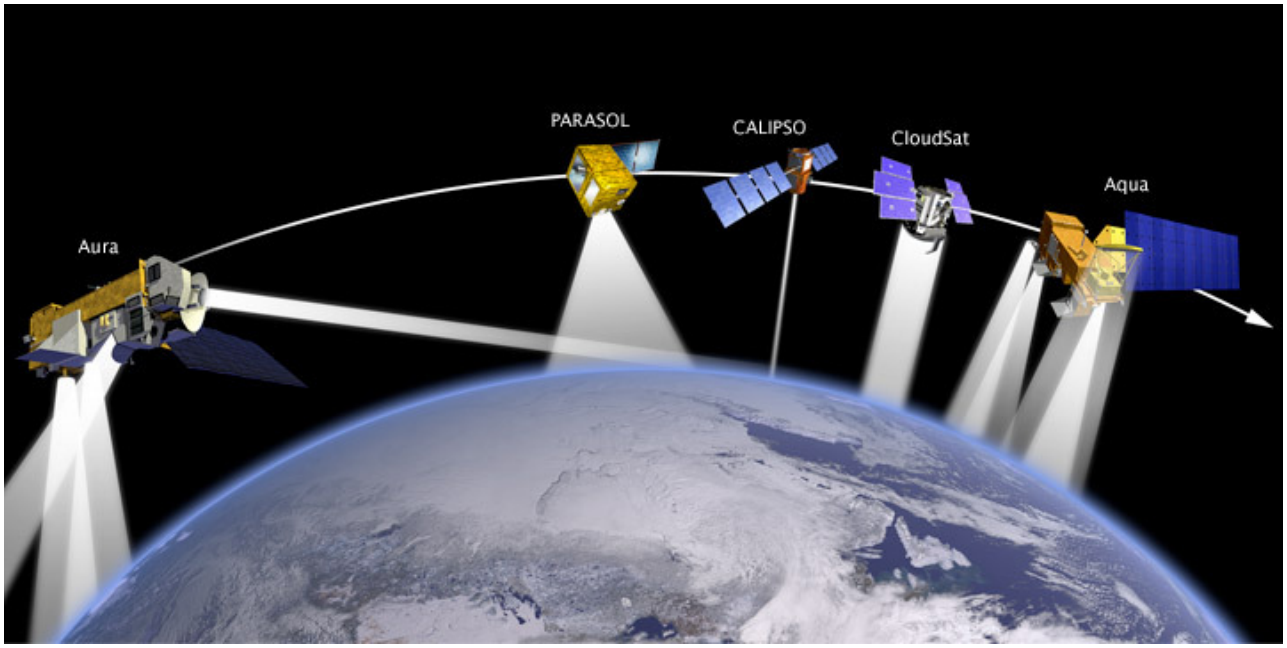

Figure 1.3: A graphic depicting the satellites that make up the A-train. [Graphic taken from NASA, 2010.]

Aqua

Aqua, sometimes referred to by the pre-launch name EOS PM-1, was launched on 4th May 2002 [Parkinson, 2003]. Like Terra, it is has CERES and MODIS instruments onboard, in addition to AIRS (Atmospheric Infrared Sounder), AMSR-E (Advanced Microwave Scanning Radiometer for the Earth Observing System), AMSU-A (Advanced Microwave Sounding Unit-A) and HSB (Humidity Sounder for Brazil). Aqua flies in a sun-synchronous orbit with a northwards equatorial crossing time of 1:30 P.M.. It is the first member, with respect to both launch date and orbital position, of the afternoon A-Train constellation of satellites (Figure 1.3). These satellites fly in close formation, so there is potential to combine data from different instruments in order to produce improved data products [e.g. Jeong and Hsu, 2008].

PARASOL

Another member of the A-train, Polarization and Anisotropy of Reflectances for Atmospheric Sciences coupled with Observations from a Lidar (PARASOL), was launched on 18th December 2004 [CNES, 2009b]. It caries a POLDER (POLarization and Directionality of the Earth's Reflectances) instrument.

CloudSat

CloudSat, also part of the A-Train, was launched on 28th April 2006, and carries the first satellite Cloud Profiling Radar (CPR) [Colorado State University, 2009].

CALIPSO

The Cloud Aerosol Lidar and Infrared Pathfinder Satellite Observation (CALIPSO) satellite, another part of the A-Train, was also launched on 28th April 2006 [CNES, 2009a]. The payload consists of CALIOP (Cloud-Aerosol LIdar with Orthogonal Polarization), IRR (Imaging Infrared Radiometer) and WFC (Wide Field Camera), all co-aligned [NASA, 2009a].

1.2.2 Satellite instrumentation

ATSR, ATSR-2 and AATSR

The Along-Track Scanning Radiometer (ATSR) was launched on ERS-1; ATSR-2 is on ERS-2; the Advanced Along-Track Scanning Radiometer (AATSR) is on ENVISAT [RAL, 2003]. The primary purpose of ATSR is to measure sea-surface temperatures [Mutlow, 1993]. However, the Global Retrieval of ATSR cloud Parameters and Evaluation (GRAPE) project [University of Oxford, 2009a] is developing a retrieval scheme capable of retrieving aerosol and cloud parameters (Oxford-RAL Aerosol and Cloud, ORAC [University of Oxford, 2009b]). A new aerosol algorithm has now been developed for AATSR [Sayer, 2008].

MODIS

The MODerate resolution Imaging Spectroradiometer (MODIS) has 36 bands in the visible and infrared, with nadir resolutions of 250–1000 m, and has a cross track swath width of 2330 km [Barnes et al., 1998]. There are MODIS instruments on both Terra and Aqua. They provide complete global coverage every 1–2 days [NASA, 2009f]. Terra MODIS data from 24th February 2000 – present and Aqua MODIS data from 3rd July 2002 – present are available [NASA, 2009c]. MODIS atmospheric data products include aerosol and cloud properties, as well as water vapour [NASA, 2009e]. MODIS also provides land data, such as vegetation indices [Huete et al., 2002], and ocean data, such as chlorophyll concentration [Esaias et al., 1998].

MISR

The Multi-angle Imaging SpectroRadiometer (MISR), on Terra, images the Earth in nine different view directions [Diner et al., 1998]. It can provide cloud height data, in addition to other cloud and aerosol properties [NASA, 2009d]. The swath width is 360 km.

POLDER-1, POLDER-2 and PARASOL

The POLarization and Directionality of the Earth's Reflectances (POLDER) instrument, designed to measure polarized and directional reflected solar radiation, has a swath width of approximately 2200 km and a resolution of 6×7 km^2 [Deschamps et al., 1994]. Measuring polarized and directional reflectances allows it to differentiate between radiation scattered in the atmosphere and that reflected by the Earth's surface, allowing improved observations of clouds, aerosols, the land surface and oceans [CNES, 2009c]. Data are available from three POLDER instruments: POLDER-1, on ADEOS-1, from November 1996 – June 1997; POLDER-2, on ADEOS-2, from April 2003 – October 2003; the third POLDER instrument, on PARASOL, from December 2004 onwards [Université Lille 1, 2009]. PARASOL is intended to observe clouds and aerosols [CNES, 2009b].

CloudSat CPR

The CloudSat Cloud Profiling Radar (CPR) operates at 94-GHz (3 mm wavlength), has a horizontal footprint of 1.4 km $\times$ 3.5 km and has a vertical resolution of 250 m [Posselt et al., 2008]. It measures several cloud parameters, and a cloud classification product is available.

CALIOP

The Cloud-Aerosol LIdar with Orthogonal Polarization (CALIOP), on CALIPSO, has been producing cloud and aerosol data since 2006, much of which has a horizontal resolution of 330 m and a vertical resoltion of 30–60 m [Winker et al., 2007].

1.2.3 Assessment of using satellite data for aerosol-cloud studies

In comparison to field campaigns, which provide datasets limited in both spatial and temporal extent, satellite sensors can provide global datasets extending over several years. Although AERONET releases aerosol data retrieved at many locations on Earth, the coverage is severely limited compared to that of many satellite datasets. The large datasets offered by satellite instruments are invaluable for statistical studies of the atmosphere and the processes which occur there.

However, satellites have a number of limitations. Cloud profiling radars, such as that onboard CloudSat, and lidars, such as CALIOP, can provide vertically resolved cloud and aerosol data, but they resolve only one horizontal dimension; radiometers, such as MODIS, often have large two-dimensional horizontal coverage but generally have no vertical resolution when retrieving aerosol and cloud properties. One limitation of particular interest here is that radiometers cannot retrieve both aerosol and cloud properties simultaneously: if a pixel is identified as cloudy, a cloud retrieval will be attempted; if a pixel is identified as cloud-free, an aerosol retrieval will be attempted. So retrieved aerosol and cloud properties are never completely co-located horizontally[1]. Also, radiometer products rarely allow vertical co-location to be tested: retrieved cloud properties are often that of the top of the highest layer of cloud and may not be representative of cloud below; retrieved aerosol properties are often column averages or totals and do not provide information on the location of the aerosol, which may be in defined layers.

1.2.4 Choice of satellite data

For large-scale statistical studies of aerosols and clouds, datasets providing extensive horizontal coverage are highly desirable. Several satellite radiometers fulfil this criterion. MODIS data are available at two overpass times (Terra 10:30 A.M.; Aqua 1:30 P.M.), the data cover several years, the spatial resolution is high and the swath is wide compared to many radiometers. MODIS aerosol and cloud products have undergone several validation and comparison studies [e.g Remer et al., 2005, Wu et al., 2009], and these products are commonly used in aerosol–cloud interaction studies (see Section 1.4). We have therefore chosen to use MODIS data at the beginning of this research, although data from other satellite sensors may also be used at a later stage. Since Aqua is in the A-Train, data from other A-Train instruments could readily be used in combination with Aqua MODIS.

1.2.5 Retrieved aerosol and cloud properties

Many aerosol and cloud properties are retrieved using satellite radiometer data. Some of the commonly retreived properties which are of particular interest when investigating aerosol–cloud interactions are as follows: *aerosol optical depth* (AOD) is the total extinction at a given wavelength due to aerosol in an atmospheric column; *aerosol index* (AI) is another measure of aerosol load in an atmospheric column; *liquid cloud droplet effective radius* ($\mathrm{CER_{liquid}}$) is a retrieved estimate of the size of the droplets near the top of liquid water clouds; *liquid water path* (LWP) is the total mass of liquid water in an atmospheric column; *cloud optical depth* (COD) is the total extinction at a given wavelength due to cloud water (liquid, ice or both) in an atmospheric column; *cloud fraction* (CF) gives the total fractional cover of all clouds (liquid and ice) in a given region; *cloud top pressure* (CTP) is the average pressure at the top of all clouds (liquid and ice) in a given region.

[1] This is not completely true. By using PARASOL data together with other data from the A-train, Waquet et al. [2009] have demonstrated that it may sometimes be possible to retrieve properties of aerosols above clouds.

Although not a directly retrieved quantity, *cloud droplet number concentration* (CDNC), N_d, is sometimes estimated using the adiabatic approximation [Brenguier et al., 2000, Quaas et al., 2006]:

$$N_d = \gamma {\tau_c}^{\frac{1}{2}} {r_e}^{-\frac{2}{5}} \tag{1.1}$$

where τ_c is COD, r_e is $\text{CER}_{\text{liquid}}$ and $\gamma = 1.37 \times 10^{-5}$ $\text{m}^{-\frac{1}{2}}$.

1.3 Modelling tools

1.3.1 General circulation models and parameterization uncertainties

Modern climate prediction, like weather forecasting, relies heavily on complex numerical models used to simulate the Earth's atmosphere-ocean system [Meehl et al., 2007]. There are a number of state-of-the-art models which couple a dynamic ocean to a dynamic atmosphere, so-called *general circulation models* (GCMs), currently being used by different research facilities around the world [see e.g. Table 8.1 of Randall et al., 2007]. Each model simulates physical processes slightly differently.

Many physical processes, such as cloud formation, occur on scales too small to be resolved by GCMs, so these processes must be parameterized [e.g. Arakawa, 2004]. There is a wide range of potentially valid parameter values that can be employed for a given GCM [Randall et al., 2007]. One technique that is regularly used in probabilistic climate forecasting is to run an experiment using several different GCMs, generating a *multi-model ensemble* [e.g. Lambert and Boer, 2001]. An alternative approach is to vary the values of parameters in a single model, testing different parameter combinations, generating a *perturbed physics ensemble* [e.g. Stainforth et al., 2005, Piani et al., 2005]. Unfortunately, generating even modest-sized ensembles for a given experiment can be computationally expensive.

Climate*prediction*.net is a distributed computing project, using volunteers' computers distributed around the world to generate large perturbed physics ensembles for a number of climate experiments [Stainforth et al., 2002]. Using climate*prediction*.net data, Sanderson et al. [2008b] find that the response to greenhouse-gas forcing is dependent on two climate feedbacks largely regulated by two parameters: the *entrainment coefficient*, associated with the cloud convection parametrization, and the *ice fall speed*, which affects cloud cover and humidity. Much of the variation in *climate sensitivity*, the equilibrium temperature response for a doubling of atmospheric carbon dioxide, also appears to be due to parameters associated with clouds [Sanderson et al., 2008a].

Bony and Dufresne [2005] demonstrate that marine boundary layer clouds are a dominant source of uncertainty in tropical cloud feedbacks in GCMs. A review by Stephens [2005] highlights that much of the uncertainty in model projections of climate change is due to cloud feedbacks in models. Much work needs to be done in order to improve cloud parameterizations in GCMs, and hence improve predictions of future climate.

1.3.2 Using general circulation models for aerosol–cloud studies

Many GCMs have aerosol and cloud modules which attempt to simulate aerosol indirect effects [Penner et al., 2006]. Unlike the real atmosphere, it is often possible to switch GCM microphysics components on or off. This can allow the reasons for correlations between aerosol and cloud properties to be probed [e.g. Lohmann et al., 2006].

1.3.3 Cloud models and large-eddy simulations

Due to the computational expense of running simulations on a global scale, GCMs cannot normally be run at a high enough resolution to resolve cloud processes such as convection, so clouds must be parametrized. However, numerical models have been designed to explicitly simulate individual clouds. For example, Altaratz et al. [2008] use an axisymmetric model with high radial and vertical resolutions of 50 m, and a domain size of 4000 m in the radial direction and 5000 m in the vertical. Cloud-scale convection can be explicitly analysed and the effects of detailed microphysics schemes can be tested.

Large-eddy simulations are capable of resolving large-scale turbulence but require small-scale turbulence to be parametrized [Jacobson, 2005].

1.4 Published aerosol–cloud interaction studies

Aerosol effects on clouds and their potential significance to the climate system are currently poorly understood, as shown in Section 1.1. Much work needs to be done in order to improve our understanding of these effects. Several studies investigating interactions between observed cloud and aerosol properties have been published in recent years. We provide a brief survey of the findings of some of these studies, categorising them according to potential aerosol–cloud interactions and implications.

It is worth noting from the outset that an observed correlation between an aerosol property and a cloud property may not necessarily be due to aerosol effects on the cloud. We explore potential explanations for spurious correlations in Section 1.5.

1.4.1 Cloud albedo effect: CDNC and CER_{liquid}

Conceptually, the cloud albedo effect predicts that higher aerosol loads should lead to higher liquid cloud droplet number concentrations (CDNC) and smaller liquid cloud droplet effective radii (CER_{liquid}).

Quaas et al. [2008] find that higher MODIS AODs are generally associated with a higher CDNC (calculated using Equation 1.1). Similarly, a surface remote sensing and in situ study has shown that, for stratus clouds off the Californian coast, a positive correlation between AOD and CDNC exists [McComiskey et al., 2009].

Selecting North Atlantic stratiform clouds, Kaufman et al. [2005] find a negative correlation between CER_{liquid} and AOD in MODIS gridded daily data.

Using Along Track Scanning Radiometer ATSR-2 data for different regions and seasons, Bulgin et al. [2008] generally observed negative correlations between CER_{liquid} and AOD, although positive correlations were also often observed.

Kiran et al. [2009] claim that a decrease in CER_{liquid} observed during break spells in the indian monsoon is due to an increase in aerosol transportation to the continental tropical convergence zone during the break spells.

Using POLDER satellite data, Bréon et al. [2002] observe a negative correlation between CER_{liquid} and aerosol index (AI).

Suzuki et al. [2008] show that negative correlations exist between CER_{liquid} and AI for different liquid water clouds in data produced by NICAM-SPRINTARS (Nonhydrostatic Icosahedral Atmospheric Model - Spectral Radiation-Transport Model for Aerosol Species), a global cloud resolving model with a horizontal resolution of 7 km coupled with an aerosol transport model. They show that these findings are consistent with similar results observed in MODIS data.

Menon et al. [2008] compare aerosol-cloud relationships observed in MODIS and CERES satellite data with those produced by the GISS (Goddard Institute for Space Studies) GCM. They run three

GCM simulations: one with no aerosol microphysical effects on clouds; one with aerosol microphysical effects on low-level liquid clouds; one with winds nudged to reanalysis data, in addition to the microphysical effects. They observe that CER_{liquid} decreases with increasing AOD in the satellite data. A similar relationship, although weaker, is present in the data from GCM runs which include aerosol–cloud microphysical effects.

1.4.2 Cloud lifetime effect: LWP and CF

Conceptually, the cloud lifetime effect predicts that, due to the suppression of precipitation, a positive correlation should exist between liquid water path (LWP) and AOD. Increased cloud lifetime should also lead to a positive correlation between cloud fraction (CF) and AOD. Although the cloud lifetime effect is associated with suppression of precipitation and cloud height, these are discussed later.

Using MODIS gridded daily mean data, Koren et al. [2005] find a positive correlation between CF and AOD for convective clouds over the North Atlantic Ocean. However, using the ECHAM4 GCM and running a simulation with aerosol microphysical effects on clouds switched off, Lohmann et al. [2006] demonstrate that much of this increase in CF associated with high AOD conditions may be due to dynamical rather than microphysical effects.

The study by Menon et al. [2008] (see above) finds that for the MODIS and CERES data, high AOD conditions correspond to high CF. However, the nudged GISS GCM simulation results suggest that much of this correspondence may due to synoptic conditions.

Surprisingly, the study by Suzuki et al. [2008] (see Section 1.4.1) suggests that LWP may decrease slightly with increasing AI, a relationship observed in both the MODIS and NICAM-SPRINTARS data. This is inconsistent with the basic conceptual model of the cloud lifetime effect.

Using a single cloud model and LESs, Jiang et al. [2006] find that aerosols may increase the lifetime of shallow cumulus clouds. However their study suggests that, in addition to suppressing precipitation, smaller droplets can also lead to increased evaporation which would act to reduce the lifetime of the cloud. In some situations, it is therefore possible that an inverse cloud lifetime effect may sometimes occur.

Long-term trends in global cloud cover have been observed, although it may be unlikely that these trends are due to aerosol effects [Warren et al., 2007].

1.4.3 Aerosol effects on precipitation and CTP

Rosenfeld and Lensky [1998] observe that precipitation-forming processes appear to be different for marine and continental convective clouds, and that marine clouds are modified as they move inland into more continental aerosol conditions. They also find that high aerosol conditions, due to biomass burning and urban air pollution, can significantly suppress precipitation. Air pollution has been observed to completely inhibit precipitation in some cases [Rosenfeld, 2000].

However, Khain et al. [2005], who use a non-hydrostatic two-dimensional cloud model to investigate the dynamical effects of aerosols on clouds, conclude that sometimes aerosols can enhance convection and lead to the formation of squall lines and intense precipitation.

An in situ aircraft study over the Amazon [Andreae et al., 2004] found that smoke aerosols decrease cloud droplet sizes and suppress precipitation. As a result, clouds could extend to greater heights, transporting water, aerosols and latent heat higher in the atmosphere, and leading to an increase in thunderstorms and hail. Rosenfeld et al. [2008] provide a similar conceptual model as to why increased cloud condensation nuclei concentrations can suppress precipitation in some clouds but enhance convection and precipation in other clouds (Figure 1.4).

The findings of Meskhidze et al. [2009], who use Terra and Aqua MODIS data to look at morning–afternoon differences, support the theory that aerosols may enhance convection over the Amazon.

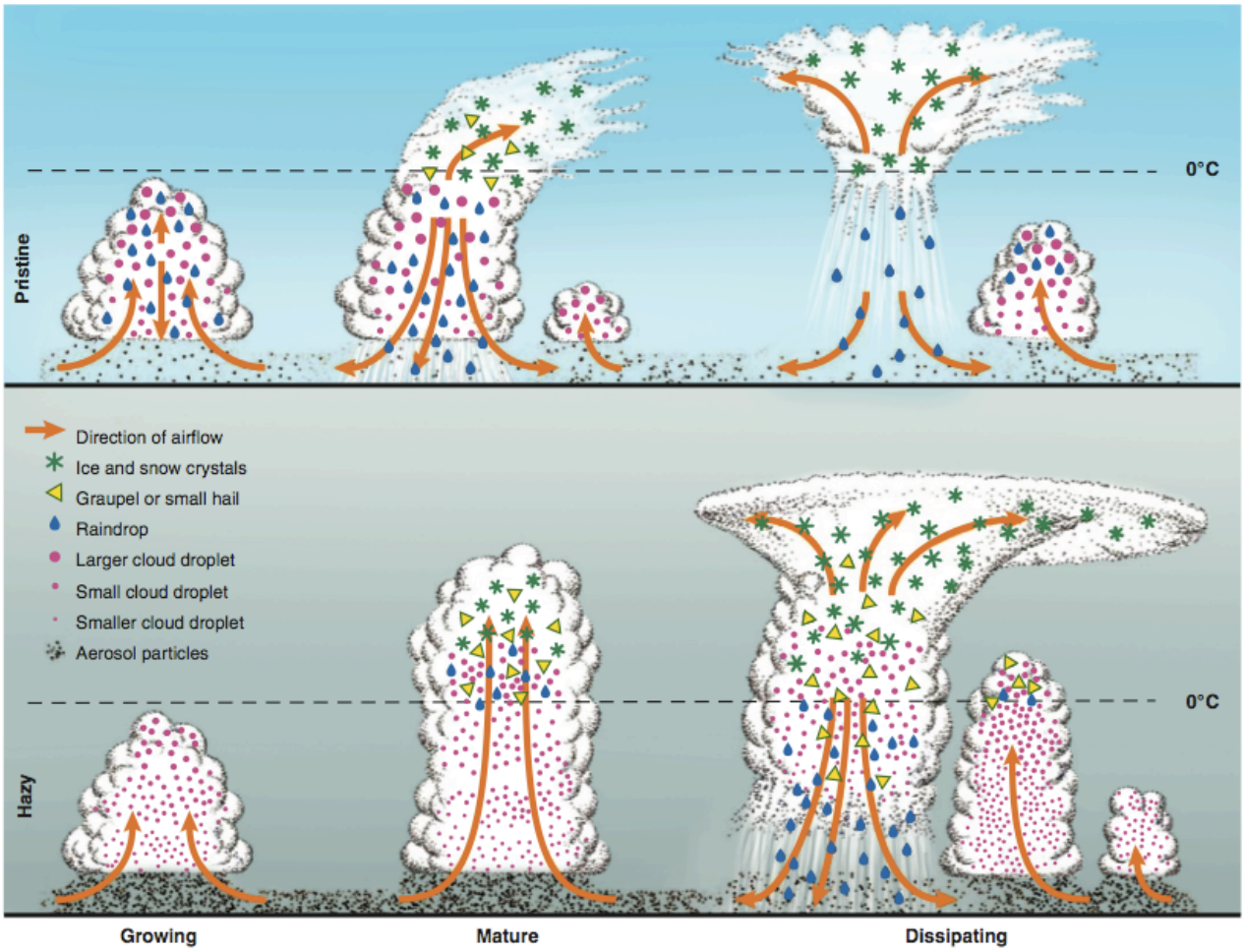

Figure 1.4: Conceptual hypothesis of the evolution of deep convective clouds developing in the pristine (top) and polluted (bottom) atmosphere. Cloud droplets coalesce into raindrops that rain out from the pristine clouds. The smaller drops in the polluted air do not precipitate before reaching the supercooled levels, where they freeze onto ice precipitation that falls and melts at lower levels. [Figure taken from Rosenfeld et al., 2008.]

Koren et al. [2005] (see Section 1.4.2) find a negative correlation between CTP and AOD, suggesting that suppression of precipitation may allow convective clouds to extend to greater heights in the North Atlantic.

1.4.4 Local aerosol effects with a global scope

Andreae et al. [2004] (see Section 1.4.3) suggest that the suppression of precipation in the Amazon could affect the global circulation and water cycle. An ECHAM4 GCM study by Nober et al. [2003] supports the idea that the suppression of precipitation and enhancement of convection by aerosols can affect the global circulation.

Other mechanisms may exist by which aerosol effects could have a global scope. Evan et al. [2008] use satellite observations and a simple model to investigate how aerosol changes have affected cyclone development in the tropical Atlantic. They argue that a reduction in aerosol direct radiative forcing would lead to higher sea-surface temperatures which could result in an increased frequency of tropical cyclones. Since tropical cyclones probably play an important role in regulating stratospheric humidity [Romps and Kuang, 2009], they may in turn affect climate and stratospheric ozone [Shindell, 2001].

1.4.5 Relative humidity and the direct effect

Interactions between aerosols and clouds may also be indirectly contributing to underestimates of direct aerosol radiative forcing. AOD has been observed to increase near clouds in both photometer and MODIS data, although MODIS retrievals may not be accurate in such cases [Redemann et al., 2009]. This increase is most likely due to the swelling of aerosols in the high humidity environments near clouds. Koren et al. [2007] argue that satellite measurements of AOD are biased towards cloud-free environments, and these measurements are therefore unrepresentatively low because they do not include scenes where aerosols are hygroscopically large in the high humidity environments near clouds. Using aircraft observations collected during the Indian Ocean Experiment (INDOEX), Twohy et al. [2009] provide evidence that relative humidity effects on aerosols in the vicinity of clouds can lead to a 35–65 % enhancement in direct radiative forcing, and that this is not properly accounted for in global radiative forcing estimates.

1.4.6 Dependence on specific conditions

Predicting how a cloud will respond to aerosol is complicated.

Cui et al. [2006] conducted a study using an axisymmetric model of a mixed phase convective cloud in low wind-shear continental conditions and found that increasing aerosols led to stagnated cloud development, a lower cloud top, weaker updrafts and suppressed precipitation. They mention that cloud response to aerosols appears heavily dependent on the type of cloud and conditions.

Using a numerical model of convective clouds, Altaratz et al. [2008] show that aerosol effects are dependent on relative humidity conditions.

Jones et al. [2009], who use MODIS data together with reanalysis data, suggest that synoptic conditions, aerosol type and the vertical location of an aerosol layer may be much more significant factors than AOD.

Using MODIS satellite and SPRINTARS model data, L'Ecuyer et al. [2009] suggest that sulphate and sea-salt aerosols may have opposite effects on clouds: sulphate aerosol can decrease precipitation and enhance vertical development, whereas sea-salt can increase precipitation and supress vertical development. This is probably because hydrophilic sea-salt can act as a giant cloud condensation nucleus on which large droplets can grow.

1.5 Possible reasons for spurious aerosol–cloud relationships

Many relationships between aerosols and cloud properties have been observed, and many potential implications have been suggested in recent years. However, the observed relationships are not necessarily due to causal relationships between aerosols and clouds. They may be due to erroneous satellite data, spatiotemporal climatological factors and meteorological effects.

1.5.1 Satellite data errors

Satellite datasets are not completely reliable. One potential problem of interest here is that of cloud-flagging errors associated with false identification of cloud or aerosol. Thin cloud, which may well be in a broken cloud field, may be flagged as cloud-free and a high AOD may therefore be retrieved, resulting in a false correlation between high AOD conditions and cloud cover.

Another problem is that retrievals are not always accurate. Bréon and Doutriaux-Boucher [2005] find a poor correlation between MODIS and POLDER CER_{liquid} over land, with a better correlation over ocean, although MODIS CER_{liquid} is generally higher. Polder is limited to homogeneous cloud fields. Marshak et al. [2006] suggest that the MODIS CER_{liquid} retrieval may not be reliable for inhomogeneous cloud fields.

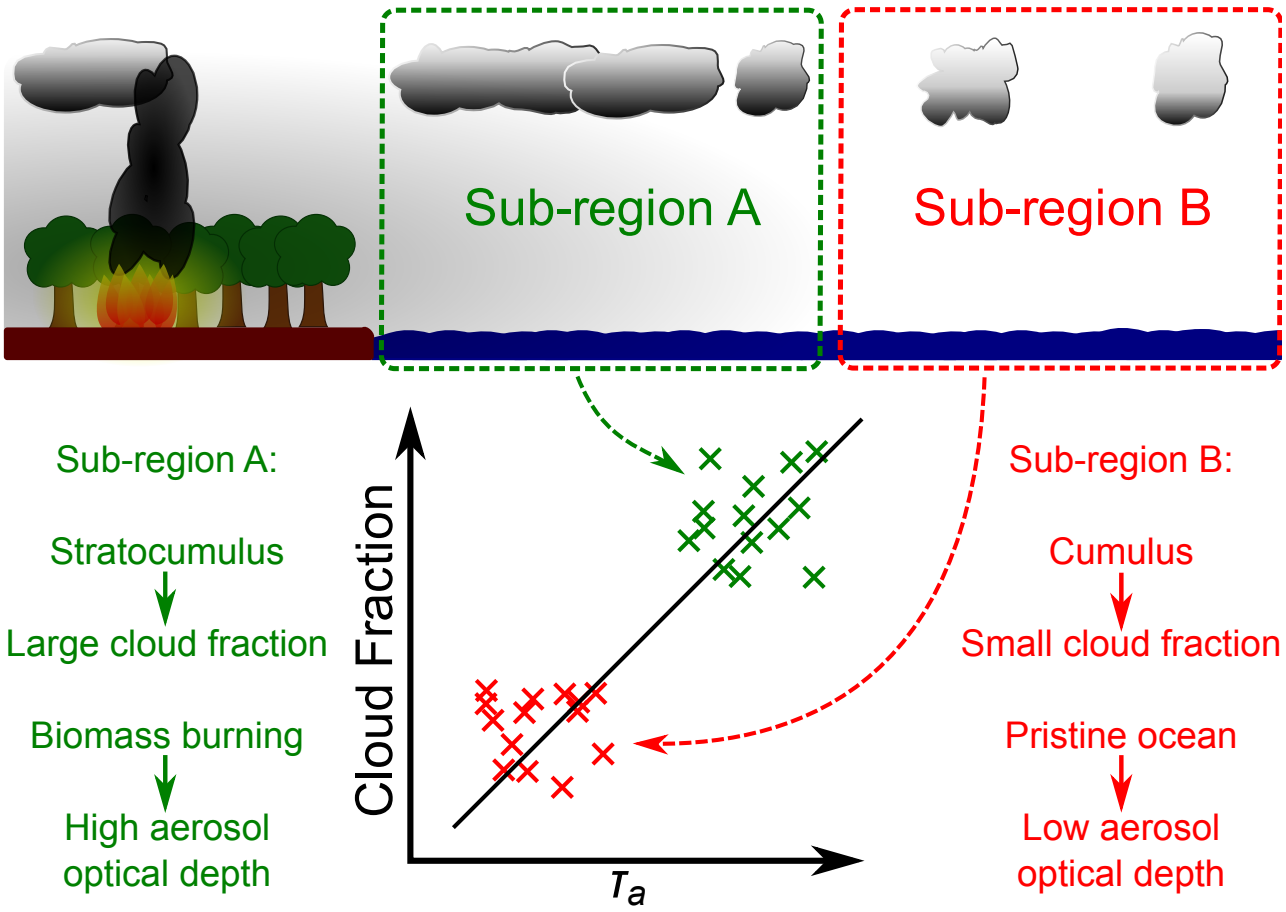

Figure 1.5: A schematic illustrating a hypothetical ocean region comprising two hypothetical sub-regions (sub-region A and sub-region B). Sub-region A is characterised by stratocumulus cloud and biomass burning aerosol; sub-region B is characterised by cumulus cloud in a pristine ocean environment. No statistically significant relationship between aerosol and cloud properties exists within each sub-region. However, analysing data for both sub-regions together leads to the spurious observation that high AOD τ_a generally corresponds to a large cloud fractional coverage, as show in the scatter plot.

1.5.2 Spatiotemporal climatological effects

Many regions of the world experience seasonal changes which may include pronounced seasonal cycles of aerosol and cloud properties. Many studies already aim to remove this temporal climatological factor by looking at individual seasons.

Similarly, different regions experience different climatological conditions. This may lead to spurious correlations between aerosol and cloud properties. Figure 1.5 illustrates a hypothetical ocean region with two sub-regions: one characterised by low thin stratocumulus cloud and biomass burning aerosol; the other, more remote, characterised by thicker fragmented cumulus cloud and sea-salt aerosol with a generally lower AOD. One potential spurious correlation introduced by treating the two sub-regions as one larger region would be the observation that higher AOD corresponds to thinner clouds with a lower CF, relationships which may exist in neither of the sub-regions if they were to be analysed in isolation. Such spatial climatological effects are discussed further in Chapter 2.

1.5.3 Meteorological effects

Even if all large-scale climatological factors are correctly accounted for, smaller scale meteorological effects may also lead to spurious correlations between aerosol and cloud properties.

As mentioned in Section 1.4.5, aerosols often swell hygroscopically in high humidity conditions, significantly increasing AOD. Since clouds also occur in high relative humidity environments, this could lead to spurious correlations between AOD and cloud properties [Quaas et al., 2010].

It is also possible that synoptic conditions may often lead to spurious correlations between aerosols and clouds. Extratropical cyclones and fronts, examples of synoptic systems, are discussed further in Chapter 3.

1.6 Aims of this project

The primary aim of this project is to improve our quantitative understanding of aerosol–cloud interactions and their role in the Earth's climate system. By developing new methods of analysing available satellite data, some of the possible reasons for observed relationships between aerosol and cloud properties will be explored. Two major areas of focus will be the role of spatial climatologies and the role of synoptic conditions.

Chapter 2

A critical look at spatial scale choices in satellite-based aerosol indirect effect studies

The text and figures in this chapter are those of Grandey and Stier [2010] (B. S. Grandey and P. Stier. A critical look at spatial scale choices in satellite-based aerosol indirect effect studies. *Atmos. Chem. Phys. Discuss.*, 10:15417–15440, 2010. doi:10.5194/acpd-10-15417-2010).

Analysing satellite datasets over large regions may introduce spurious relationships between aerosol and cloud properties due to spatial variations in aerosol type, cloud regime and synoptic regime climatologies. Using MODerate resolution Imaging Spectroradiometer data, we calculate relationships between aerosol optical depth τ_a, derived liquid cloud droplet effective number concentration N_e and liquid cloud droplet effective radius r_e at different spatial scales. Generally, positive values of $\frac{\mathrm{d}\ln N_e}{\mathrm{d}\ln \tau_a}$ are found for ocean regions, whilst negative values occur for many land regions. The spatial distribution of $\frac{\mathrm{d}\ln r_e}{\mathrm{d}\ln \tau_a}$ shows approximately the opposite pattern, with generally postive values for land regions and negative values for ocean regions. We find that for region sizes larger than $4^\circ \times 4^\circ$, spurious spatial variations in retrieved cloud and aerosol properties can introduce widespread significant errors to calculations of $\frac{\mathrm{d}\ln N_e}{\mathrm{d}\ln \tau_a}$ and $\frac{\mathrm{d}\ln r_e}{\mathrm{d}\ln \tau_a}$. For regions on the scale of $60^\circ \times 60^\circ$, these methodological errors may lead to an overestimate in global cloud albedo effect radiative forcing of order 80%.

2.1 Introduction

In order to accurately forecast future warming trends, it is important to quantify present day radiative forcing due to aerosols [Andreae et al., 2005, Kiehl, 2007]. However, there is a large uncertainty in the present-day total anthropogenic radiative forcing, and much of this uncertainty is due to uncertainties in the size of indirect aerosol effects on clouds [Forster et al., 2007, Denman et al., 2007, Lohmann and Feichter, 2005].

One of these effects is the cloud albedo effect, also known as the first indirect effect. For a cloud of constant liquid water content, increasing the number of cloud condensation nuclei leads to greater competition for available water vapour, resulting in a greater number of smaller droplets. This increases the albedo of the the cloud [Twomey, 1977], resulting in more shortwave radiation being reflected to space. A strong correlation between cloud condensation nuclei concentrations and aerosol optical depth τ_a, the total extinction at a given wavelength due to aerosol in an atmospheric column, has been observed [Andreae, 2009]. This suggests that τ_a can be used as a surrogate for cloud condensation nuclei concentration.

Many observational studies looking of the cloud albedo effect have been published. Quaas et al. [2008] find that higher MODerate resolution Imaging Spectroradiometer (MODIS) τ_a is generally associated with higher liquid cloud droplet effective number concentration N_e. Similarly, a surface remote sensing and in situ study has shown that, for stratus clouds off the Californian coast, a positive correlation between N_e and τ_a exists [McComiskey et al., 2009]. Selecting North Atlantic stratiform clouds, Kaufman et al. [2005] find a negative correlation between MODIS gridded daily τ_a and liquid cloud droplet effective radius r_e, a retrieved estimate of the size of the droplets near the top of liquid water clouds. Using Along Track Scanning Radiometer ATSR-2 data for different regions and seasons, Bulgin et al. [2008] generally observed negative correlations between r_e and τ_a, although positive correlations were also often observed. Kiran et al. [2009] claim that a decrease in r_e observed during break spells in the Indian monsoon is due to an increase in aerosol transport to the continental tropical convergence zone during the break spells. Using satellite data from the POLarization and Directionality of the Earth's Reflectances (POLDER) instrument, Bréon et al. [2002] observe a negative correlation between r_e and aerosol index.

However, these observed relationships are not necessarily indicative of causal microphysical effects. For example, satellite retrieval errors or meteorological effects may contribute towards the observed correlations [Stevens and Feingold, 2009].

Spatially-varying aerosol and cloud climatologies may also often contribute towards observed relationships between aerosol and cloud properties. This may affect the results of many of the aforementioned studies which analyse data on a relatively large regional scale: Bréon et al. [2002] conduct their analysis on a global scale of $360^\circ \times 105^\circ$; Kaufman et al. [2005] use North Alantic regions of order $100^\circ \times 25^\circ$; Bulgin et al. [2008] use regions of varying sizes, from $14^\circ \times 8^\circ$ to $360^\circ \times 105^\circ$; Quaas et al. [2008] use continental regions of order $100^\circ \times 40^\circ$. Aerosol type, cloud regime and synoptic regime climatologies may vary over such large-scale regions. If data are analysed for the region as a whole, false correlations may be introduced. For example, a hypothetical ocean region may contain two sub-regions: one characterised by low thin stratocumulus cloud and biomass burning aerosol; the other, more remote, characterised by thicker fragmented cumulus cloud and sea-salt aerosol with a generally lower τ_a. One potential spurious correlation introduced by treating the two sub-regions as one larger region would be the observation that higher τ_a corresponds to thinner clouds with a larger fractional coverage, relationships which may exist in neither of the sub-regions if they were to be analysed in isolation. Similarly, further spurious relationships between other cloud and aerosol properties may also be introduced by looking at large regions.

In this study, the following two questions are asked: What are sensible choices of spatial scale for aerosol–cloud interation studies? What effect may spatial scale choices have on global estimates of radiative forcing due to the cloud albedo effect?

A description of the datasets and methodology used in this study is provided in Sect. 2.2. Results are presented in Sect. 2.3 and discussed, with reference to these two questions, in Sect. 2.3.1.

2.2 Method

2.2.1 Data

The MODIS instruments, onboard the Terra [Kaufman et al., 1998] and Aqua [Parkinson, 2003] satellites, each observe the earth using 36 spectral bands [Barnes et al., 1998]. Using these radiances, aerosol and cloud properties are often retrieved. This study uses MODIS Science Team collection 5 daily $1^\circ \times 1^\circ$ gridded level 3 products retrieved from Terra-MODIS radiances (MOD08_D3) for the ten-year period March 2000 – February 2010.

Aerosol optical depth τ_a values from the joint land and ocean mean aerosol optical depth dataset, retrieved at 550nm [Remer et al., 2005], are used here.

For liquid cloud droplet effective radius r_e, this study uses values from the quality-assured liquid cloud effective radius dataset. Retrievals of r_e may be highly unreliable. Bréon and Doutriaux-Boucher [2005] find a poor correlation between MODIS and POLDER r_e over land, with a better correlation over ocean, although MODIS r_e is generally higher. Since POLDER is limited to homogeneous cloud fields, their findings apply primarily to homogeneous cloud fields. Marshak et al. [2006] suggest that the MODIS r_e retrieval may be even less reliable for inhomogeneous cloud fields. However, a detailed discussion of r_e uncertainties is outside the scope of the current work [see e.g. Bréon and Doutriaux-Boucher, 2005, Marshak et al., 2006, Vant-Hull et al., 2007]. The MODIS r_e product has been used in other studies [e.g. Kaufman et al., 2005, Kiran et al., 2009].

Theoretical considerations predict that, for constant liquid water path w, the cloud albedo effect E_r with respect to r_e can be written as

$$E_r = -\left.\frac{\partial \ln r_e}{\partial \ln \tau_a}\right|_w \tag{2.1}$$

[Feingold et al., 2001]. The requirement of constant w can be removed by instead considering the cloud albedo effect E_N with respect to N_e [Feingold et al., 2001, McComiskey et al., 2009]:

$$E_N = \frac{\mathrm{d}\ln N}{\mathrm{d}\ln \tau_a} = 3E_r. \tag{2.2}$$

Although not a directly-retrieved quantity, liquid cloud droplet effective number concentration, N_e, is sometimes estimated using the adiabatic approximation:

$$N_e = \gamma {\tau_c}^{\frac{1}{2}} {r_e}^{-\frac{5}{2}}, \tag{2.3}$$

where τ_c is cloud optical depth and $\gamma = 1.37 \times 10^{-5}$ m$^{-\frac{1}{2}}$ [Brenguier et al., 2000, Quaas et al., 2006]. This relationship assumes that liquid water content and liquid cloud droplet radius increase monotonically with height in the cloud, that the true droplet number concentration is constant and that r_e is representative of the true liquid cloud droplet radius at the top of the cloud. If these assumptions are valid, then N_e will be a good proxy for the true droplet number concentration. Further discussion about the validity of Eq. (2.3) is provided elsewhere [e.g. Kubar et al., 2009]. It is worth noting that the conclusions presented in Sect. 2.3.1 are not dependent on the validity of Eq. (2.3), and that the current work also presents results for r_e, a directly retrieved cloud property.

N_e is calculated by applying Eq. (2.3) to the liquid cloud optical thickness and effective radius joint histogram. Thin clouds are more likely to have unreliable r_e measurements, and the retrieval may be more reliable when $r_e < 4$ μm [Nakajima and King, 1990]. Following Quaas et al. [2006], clouds with $\tau_c < 4$ and $r_e < 4$ μm are excluded when calculating N_e.

2.2.2 Calculation of sensitivities

Following the method of Quaas et al. [2008], the sensitivity, b_ϕ, of a cloud property, ϕ, to τ_a is defined here as

$$b_\phi = \frac{\mathrm{d}\ln\phi}{\mathrm{d}\ln\tau_a}. \tag{2.4}$$

Of interest to this study is b_{re}, the sensitivity of r_e, (cf. Eq. (2.1)) and b_{Ne}, the sensitivity of N_e, (cf. Eq. (2.2)).

When calculating sensitivities at $1^\circ \times 1^\circ$ resolution, Eq. (2.4) is applied to data for a given season (December–January–February DJF, March–April–May MAM, June–July–August JJA or September–October–November SON) and $1^\circ \times 1^\circ$ grid box. This methodology can be thought of as calculating the linear regression slope of a scatter plot of $\ln\phi$ vs $\ln\tau_a$, where each point represents a day for

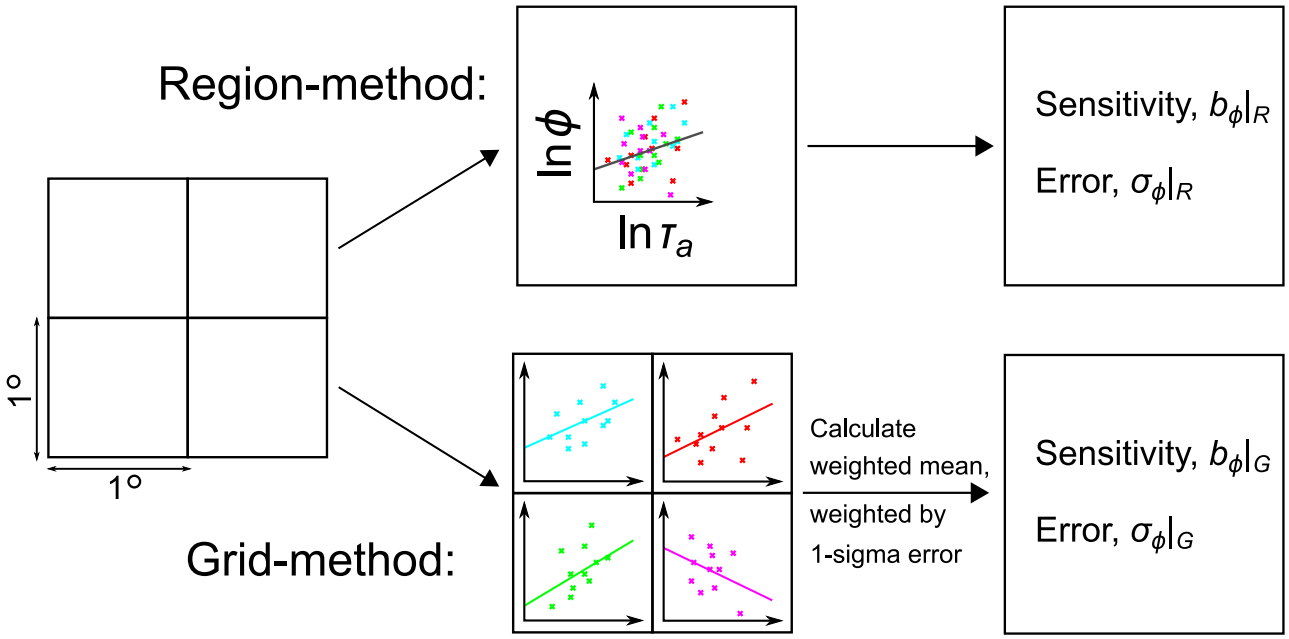

Figure 2.1: A schematic illustrating the methods used to calculate sensitivities, applied to a $2^\circ \times 2^\circ$ region. Each point in the scatter plot represents a $1^\circ \times 1^\circ$ grid box and day for which both cloud and aerosol data exist. The different colours are used to show data from different grid boxes. For simplicity, only a small number of data points are shown in this schematic.

which both aerosol and cloud data exist for this grid box. The one-sigma error of the regression fit is also calculated.

When moving to larger regions, and ultimately the globe, there are two possible ways to extend this methodology, as illustrated in Fig. 2.1. A single scatter plot for the entire region, where different points represent different combinations of date and $1^\circ \times 1^\circ$ grid box, could be considered. This is the method used by Quaas et al. [2008, 2009] and is very similar to the methods used in the studies discussed in Sect. 2.1 [Bréon et al., 2002, Kaufman et al., 2005, Bulgin et al., 2008]. This is referred to here as the region-method, and its use is indicated by a subscript R, e.g. $b_{Ne}|_R$. The region-method samples both temporal and spatial variability.

Alternatively, values of sensitivity for each individual $1^\circ \times 1^\circ$ grid box could be calculated, before calculating a mean, weighted by the one-sigma error, for the whole region. An error-weighted mean is used in order to reduce the impact of unreliable values with a large error, many of which may be outliers. This second method is referred to as the grid-method, indicated by a subscript G, e.g. $b_{Ne}|_G$. The grid-method samples temporal variability only.

As discussed in the introduction, the region-method has the potential to introduce a spurious sensitivity signal due to spurious spatial variations in cloud and aerosol climatologies. This will be demonstrated by randomly shuffling the temporal pairing of cloud and aerosol data within each season and $1^\circ \times 1^\circ$ grid box, assuming that aerosol and cloud properties for different days are independent. (See Figs. 2.2 and 2.4.) The application of this randomisation is indicated by a subscript $Rand$, e.g. $b_{Ne}|_{R,Rand}$.

A summary of the notation used in this paper is provided for reference in Table 2.1.

In order to avoid errors due to retrievals behaving differently between ocean and land, ocean and land regions are analysed separately using a $1^\circ \times 1^\circ$ land mask.

Near the poles, where surface ice exists and satellite observations are at high solar zenith angles, properties retrieved from satellite data can often be unreliable [e.g. Liu et al., 2009]. This problem is mostly avoided by limiting this study to regions between 60°N and 60°S.

Symbol	Meaning
τ_a	Aerosol optical depth
r_e	Liquid cloud droplet effective radius
w	Cloud liquid water path
τ_c	Cloud optical depth
N_e	Liquid cloud droplet effective number concentration
ϕ	A general cloud property, either r_e or N_e in this study
γ	Constant in Eq. (2.3); $= 1.37 \times 10^{-5}$ m$^{-\frac{1}{2}}$
b_ϕ	The sensitivity, $\frac{\mathrm{d}\ln\phi}{\mathrm{d}\ln\tau_a}$, of a general cloud property to τ_a
b_{Ne}	Sensitivity of N_e to τ_a
$b_{Ne}\|_R$	Sensitivity of N_e to τ_a, calculated using the region-method
$b_{Ne}\|_G$	Sensitivity of N_e to τ_a, calculated using the grid-method
$b_{Ne}\|_{R,Rand}$	Sensitivity of N_e to τ_a, calculated using the region-method after data randomisation
$b_{Ne}\|_{G,Rand}$	Sensitivity of N_e to τ_a, calculated using the grid-method after data randomisation
b_{re}	Sensitivity of r_e to τ_a
$b_{re}\|_R$	Sensitivity of r_e to τ_a, calculated using the region-method
$b_{re}\|_G$	Sensitivity of r_e to τ_a, calculated using the grid-method
$b_{re}\|_{R,Rand}$	Sensitivity of r_e to τ_a, calculated using the region-method after data randomisation
$b_{re}\|_{G,Rand}$	Sensitivity of r_e to τ_a, calculated using the grid-method after data randomisation
DJF	December–January–February
MAM	March–April–May
JJA	June–July–August
SON	September–October–November

Table 2.1: A summary of the notation used in this paper.

2.3 Results

The first column of Fig. 2.2 shows the annual mean $b_{Ne}|_R$, region-method sensitivity of N_e to τ_a, for different region sizes. The top map, for $1^\circ \times 1^\circ$ regions, shows positive sensitivities (red) over much of the ocean, indicating that higher τ_a generally corresponds with higher N_e over these areas, as predicted by the cloud albedo effect conceptual model. In contrast, negative sensitivities (blue) exist for some land areas, indicating that higher τ_a is associated with lower N_e. Much of the map is white, indicating that the calculated $b_{Ne}|_R$ values were often not statistically significantly different from zero at the two-sigma confidence level. As the region size increases, the fraction of the globe containing statisically significant $b_{Ne}|_R$ increases substantially.

For the grid-method, shown in the second column of Fig. 2.2, the statistical significance of $b_{Ne}|_G$ also improves substantially with increasing region size. The general spatial distribution of grid-method sensitivities is similar to those of the region-method, with $b_{Ne}|_G$ being mostly positive over the ocean and negative over land. However, some differences between $b_{Ne}|_R$ and $b_{Ne}|_G$ are also evident. For example, over the North-West Pacific, near East Asia, the $60^\circ \times 60^\circ$ $b_{Ne}|_R$ is much larger than $b_{Ne}|_G$.

The difference between $b_{Ne}|_R$ and $b_{Ne}|_G$ is shown in the third column of Fig. 2.2. White shows where the difference is not significantly different from zero at the two-sigma confidence level. The region-method and grid-method only diverge at scales larger than $1^\circ \times 1^\circ$, so the $1^\circ \times 1^\circ$ $b_{Ne}|_R - b_{Ne}|_G$ map shows no difference between the two methods, as expected. At $4^\circ \times 4^\circ$, differences begin to appear along some of the coasts and land areas, probably due to surface albedo changes causing spatially-varying satellite retrieval errors. At $8^\circ \times 8^\circ$, many more differences can be seen, including over ocean areas. For $15^\circ \times 15^\circ$ and $60^\circ \times 60^\circ$, the presence of significant differences increases

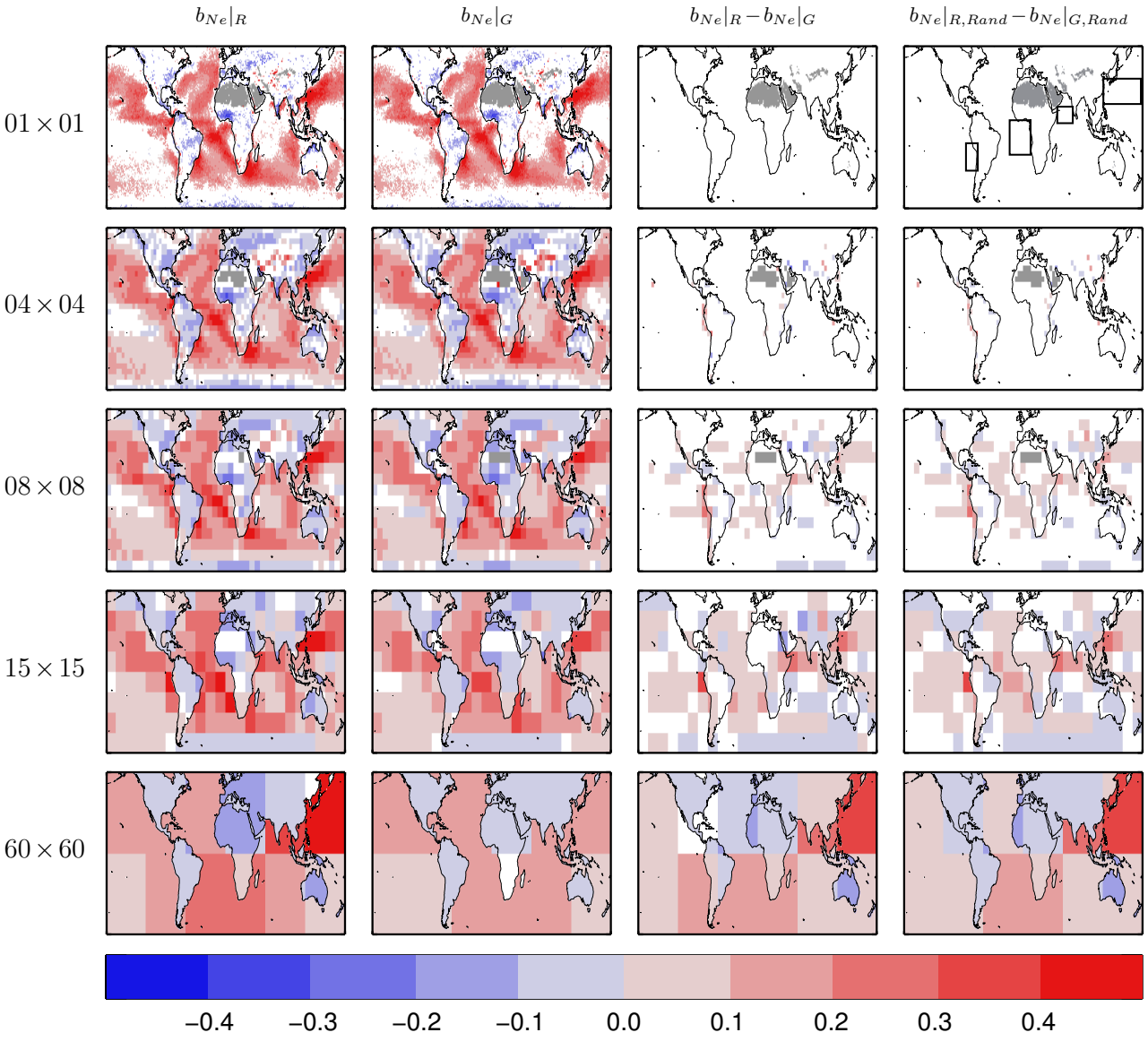

Figure 2.2: Annual mean sensitivity of N_e to τ_a for different region sizes. The first column shows the results for the region-method; the second column is for the grid-method; the third column is the difference between the region-method and grid-method sensitivities; the fourth column is the difference when the data have first been randomised within each season and $1^\circ \times 1^\circ$ grid box. White regions are where the data are not significantly different from zero at two-sigma confidence, using the error from the sensitivity regression fit. Grey represents missing data. The four rectangles in the top right hand map indicate the regions commented on in Sect. 2.3.

substantially.

In order to demonstrate that the observed differences occur due to spatial scale changes, the fourth column of Fig. 2.2 shows the difference between the region-method and the grid-method for data which has been temporally randomised within each $1^\circ \times 1^\circ$ grid box and season prior to calculationg the annual mean. This randomisation generally causes $b_{Ne}|_{G,Rand}$ to become insignificantly different from zero, with a few statistically significant departures from zero being the result of noise. The dominant signal in $b_{Ne}|_{R,Rand} - b_{Ne}|_{G,Rand}$ is due to spatially-varying changes in N_e and/or τ_a within regions, either as a result of physical climatologies or surface albedo changes affecting satellite retrievals. The strong similarity between $b_{Ne}|_{R,Rand} - b_{Ne}|_{G,Rand}$ and $b_{Ne}|_R - b_{Ne}|_G$ demonstrates that these sensitivity differences arise as a result of varying climatologies and/or surface albedo within regions.

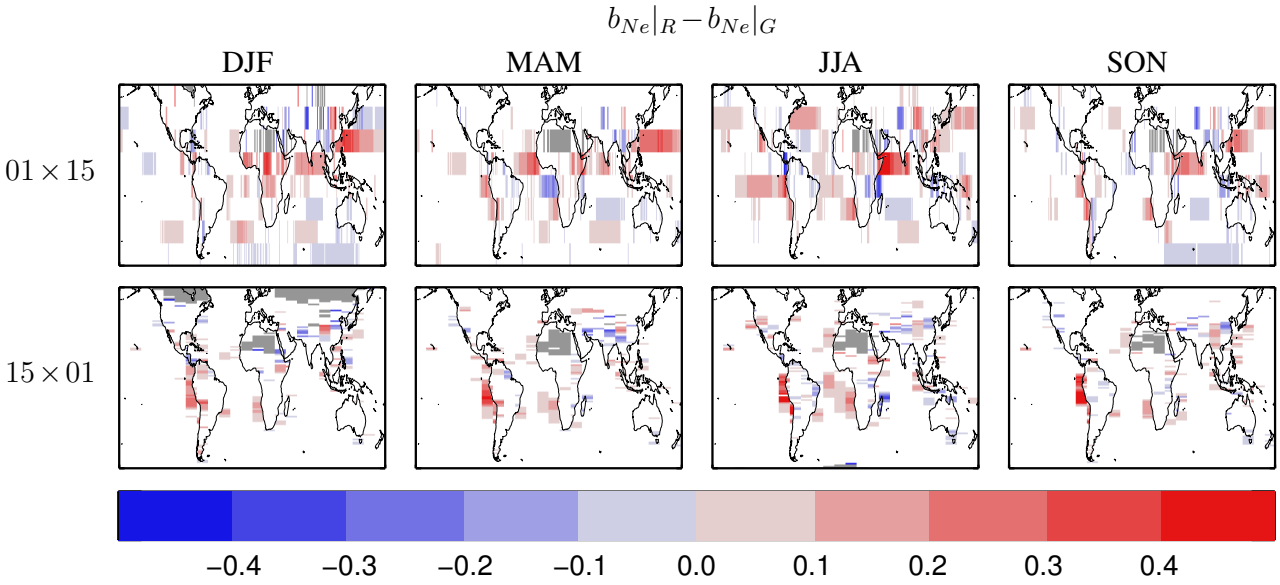

Figure 2.3: Difference in sensitivity of N_e to τ_a between the region-method and grid-method for different seasons and two different region shapes (meridional and zonal). White regions are where the data are not significantly different from zero at two-sigma confidence. Grey represents missing data.

By looking at different region shapes, it is possible to investigate whether the $b_{Ne}|_R - b_{Ne}|_G$ differences are predominantly meridional or zonal in nature. Figure 2.3 shows the difference $b_{Ne}|_R - b_{Ne}|_G$ for different seasons and two different region definitions: $1^\circ \times 15^\circ$ (meridional) and $15^\circ \times 1^\circ$ (zonal). It can be seen that both merdional and zonal changes contribute, with merdional changes being more widespread over the open ocean.

Four ocean areas are worthy of particular mention: the western North Pacific, to the east of China; the Arabian sea, between the Horn of Africa and India; the eastern South Pacific, near the South American coast; and the eastern South Atlantic, near the African coast. These four regions are indicated on the map at the top right of Fig. 2.2. Below, each of these four regions is considered briefly.

Parts of the western North Pacific, to the east of China, show a large difference between $b_{Ne}|_R$ and $b_{Ne}|_G$ at region-scales of $8^\circ \times 8^\circ$ and above (Fig. 2.2), much of which is meridional (Fig. 2.3). Aerosol properties are known to vary significantly within this region, often exhibiting a gradient in absorptivity and fine-mode fraction with distance from the coast [Choi et al., 2009]. A significant part of this variation in aerosol properties is meridional.

The Arabian sea, between the Horn of Africa and India, also shows a large meridional difference between $b_{Ne}|_R$ and $b_{Ne}|_G$, particularly during the summer months (Fig. 2.3). This area often contains airborne dust originating from dust storms, with τ_a being higher in summer than in winter [Li and Ramanathan, 2002]. The presence of dust often leads to situations where aerosol and cloud are misidentified [Brennan et al., 2005], leading to errors in retrieved properties. Since there is a strong meridional gradient in τ_a due to dust over the Arabian sea [Li and Ramanathan, 2002], this may lead to a meridionally-varying contribution of contamination to retrieved properties.

The results presented here suggest that stratocumulus region indirect effect studies may be particularly susceptible to spatial scale choices. The eastern South Pacific stratocumulus region, to the west of Peru and Chile, shows persistent differences between $b_{Ne}|_R$ and $b_{Ne}|_G$ (Figs. 2.2 and 2.3). Interestingly, the eastern South Atlantic stratocumulus region, to the west of Africa, shows a negative meridional difference in MAM but not in other seasons. Aerosol types and cloud properties are known to vary spatially within these regions [e.g. George and Wood, 2010], and variations may have a significant impact on observed aerosol indirect effects [Andrejczuk et al., 2008]. These spatial

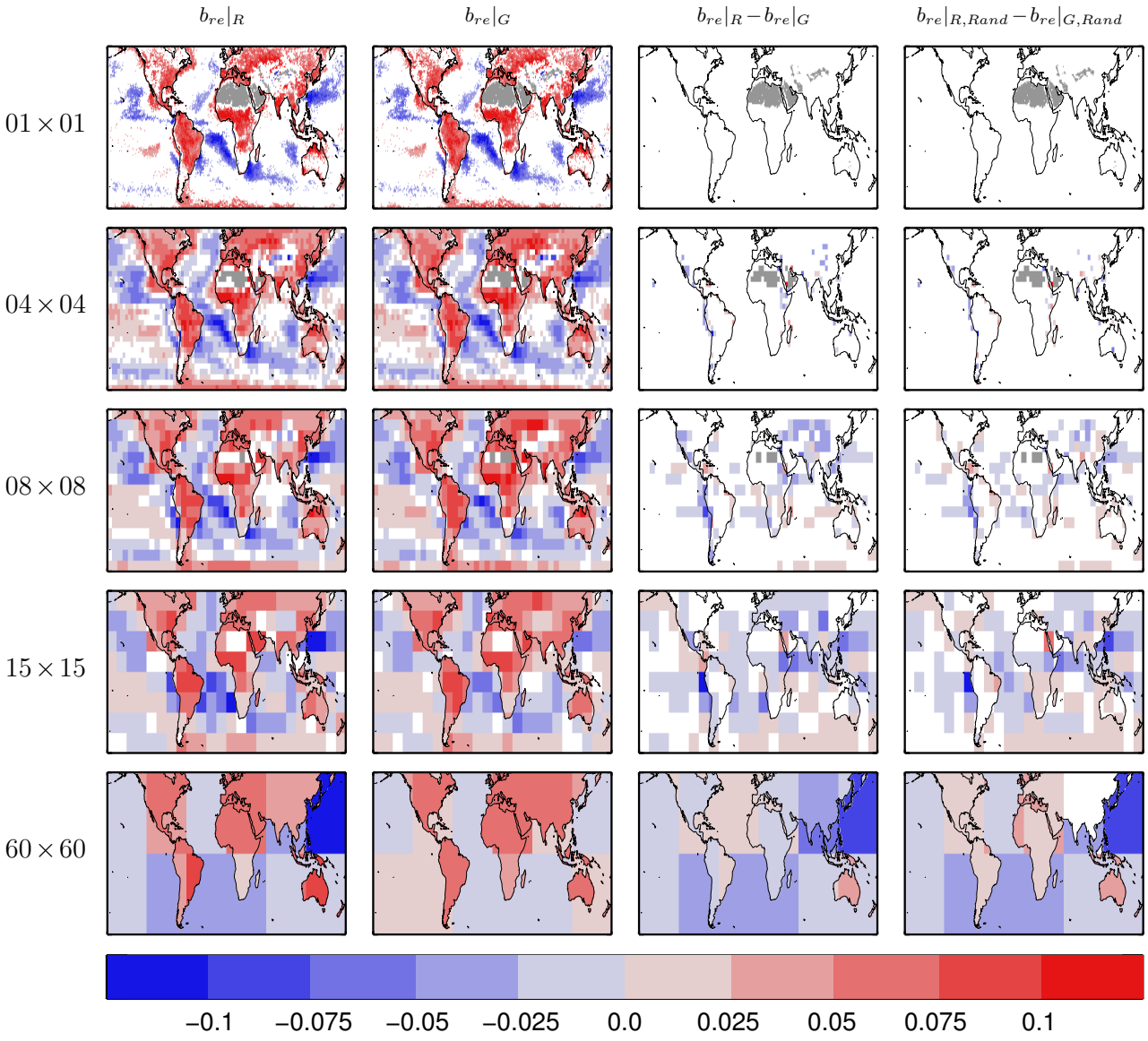

Figure 2.4: Same as Fig. 2.2, but for sensitivity of r_e to τ_a.

variations must be taken into account when studying stratocumulus regions.

Figures 2.4 and 2.5 show b_{re}, the sensitivity of r_e to τ_a, which exhibits a very similar pattern to Figs. 2.2 and 2.3, except for the inverted sign and colour bar range. For the first and second columns of Fig. 2.4, blue regions show where b_{re} is negative, indicating that higher τ_a generally corresponds with smaller droplets, and red regions show where b_{re} is positive, indicating that higher τ_a corresponds with larger droplets. The aforementioned observations concerning the sensitivity of N_e also apply to the sensitivity of r_e. For example, the third column of Fig. 2.4 shows that statistically significant differences between $b_{re}|_G$ and $b_{re}|_R$ emerge as the region size increases. These differences occur mainly along the coast and over land at $4^\circ \times 4^\circ$, but are found everywhere at $60^\circ \times 60^\circ$. As before, the fourth column shows that these differences are similar if the data have been randomly shuffled within each $1^\circ \times 1^\circ$ grid box. The four regions commented on above also show large $b_{re}|_R - b_{re}|_G$ differences in Figs. 2.4 and 2.5.

Figure 2.6 shows the relative error introduced to the global average of b_{Ne} through the use of the region-method compared to the grid-method. As expected, this error increases with region size. This error generally acts such that the region-method leads to an overestimate of b_{Ne} compared to the grid-method. For the ocean-land combined and ocean-only sensitivities, this error increases rapidly

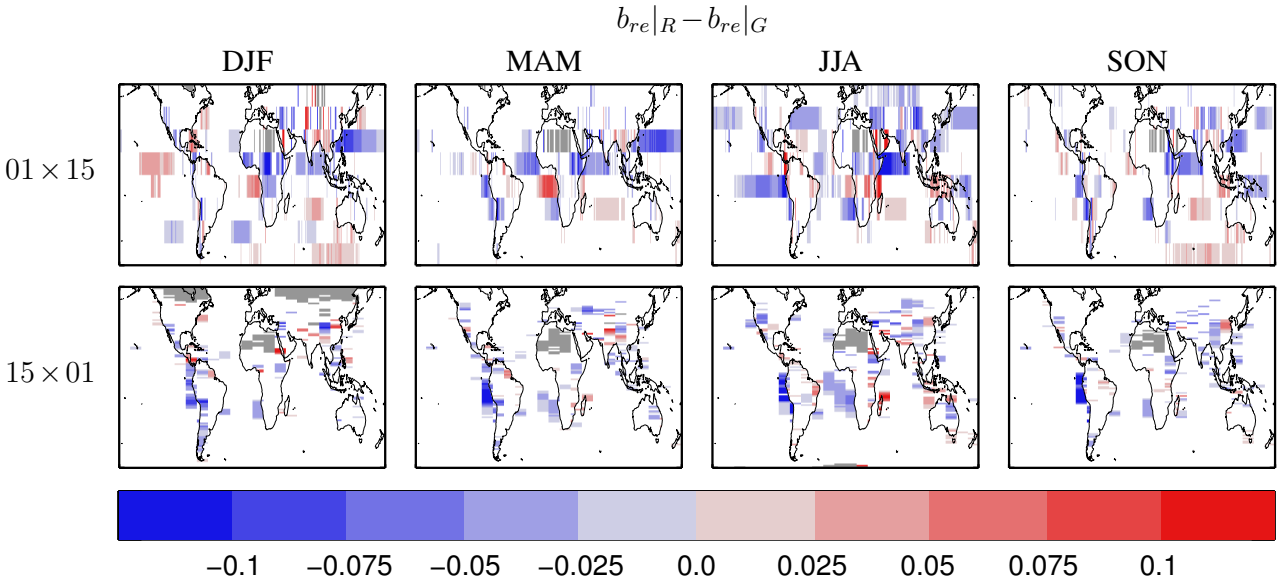

Figure 2.5: Same as Fig. 2.3, but for sensitivity of N_e to τ_a.

to ∼5–10% between $4^\circ \times 4^\circ$ and $8^\circ \times 8^\circ$. It is at this scale that statistically significant differences begin to become apparent in many individual regions, as shown in Fig. 2.2 and commented on earlier. Likewise, as can be seen in Fig. 2.7, for r_e the region-method leads to large errors in b_{re} at region scales of $8^\circ \times 8^\circ$ and larger. At $60^\circ \times 60^\circ$, the ocean-only error in b_{re} grows to $\sim 470\%$.

Errors in sensitivities arising due to the region-method will propogate into associated estimates of cloud albedo effect radiative forcing. Quaas et al. [2008] use large-scale regions, of comparable size to the $60^\circ \times 60^\circ$ regions used here, to estimate radiative forcing. Their cloud albedo effect radiative forcing scales approximately linearly with b_{Ne}. As can be seen in Fig. 2.6, the application of the region-method at $60^\circ \times 60^\circ$ gives rise to an 80% error (70% error for ocean-only). This would introduce an estimated error of approximately 80% to the Quaas et al. [2008] cloud albedo effect radiative forcing estimate, modifying their error estimate from ± 0.1 Wm^{-2} to ± 0.2 Wm^{-2}. Quaas et al. [2008] clearly acknowledge that the uncertainty of their result is likely to be larger than ± 0.1 Wm^{-2}, due to data and methodolical errors being difficult to account for. The current study helps to quantify a methodological error.

2.3.1 Conclusions

This study aimed to address the two questions stated in Sect. 2.1: What are sensible choices of spatial scale for aerosol–cloud interation studies? What effect may spatial scale choices have on global estimates of radiative forcing due to the cloud albedo effect?

In order to address these questions, the effect of calculating aerosol–cloud relationships in satellite data over a variety of region sizes from $1^\circ \times 1^\circ$ to $60^\circ \times 60^\circ$ was investigated. Using MODIS satellite data, sensitivities (Eq. (2.4)) of derived N_e to τ_a and retrieved r_e to τ_a were calculated for these different spatial scale choices.

Generally, positive values of the sensitivity of derived N_e to τ_a are found for ocean regions, whilst negative values occur for many land regions. The spatial distribution of the sensitivity of retrieved r_e to τ_a shows the opposite pattern, with generally postive values for land regions and negative values for ocean regions.

It was found that analysing datasets over large regional scales has the potential to introduce significant errors to aerosol indirect effect studies. For regions of size $4^\circ \times 4^\circ$, spatial scale errors are

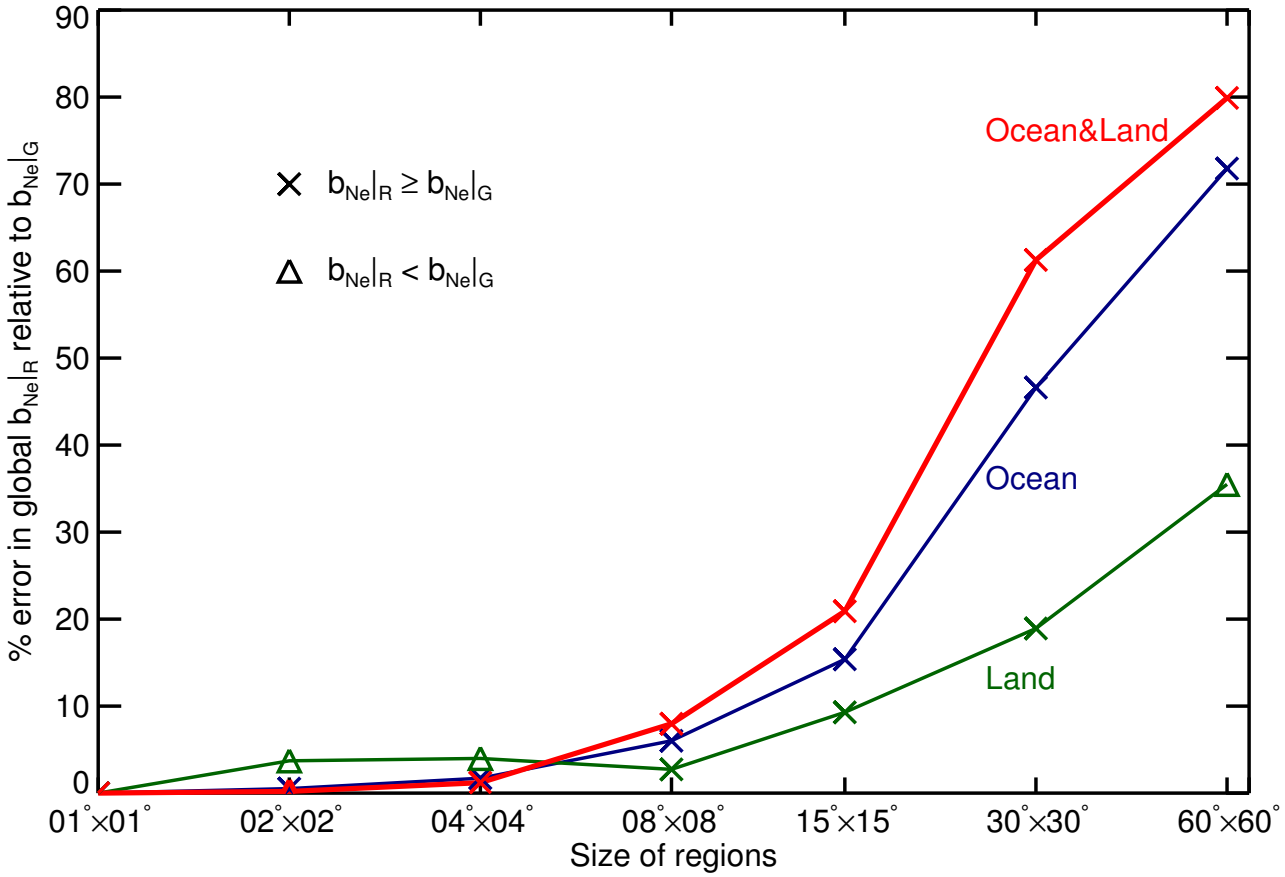

Figure 2.6: Absolute percentage error in the globally-averaged sensitivity of N_e to τ_a due to the region-method compared to the grid-method. The green data line is for land-only, the blue is for ocean-only and the red is for ocean and land combined. Crosses show where the region-method leads to an overestimate of the sensitivity (i.e. the error is positive), and triangles where the sensitivity is underestimated (the error is negative). As elsewhere in this study, weighting has been applied using the one-sigma error in the sensitivities. Latitudinal area weighting has not been applied.

generally small ($\ll 10\%$ for the sensitivity of both N_e and r_e) but often become much more significant at region sizes of $8^\circ \times 8^\circ$ and larger. At larger region scales, these errors can become much larger. For example, for regions of size $60^\circ \times 60^\circ$ the global ocean-only error in the sensitivity of r_e is $\sim 470\%$.

In light of these findings, it seems sensible to recommend $4^\circ \times 4^\circ$ as the largest size of individual regions that should be used for analysis in aerosol indirect effect studies. Caution should be applied if looking at larger regions. If data exist at a higher gridded resolution (e.g. $1^\circ \times 1^\circ$), then data should be analysed at this higher resolution. Results of calculations done at these small spatial scales can then be averaged over larger regions, allowing overall results to be calculated for large regions and the globe.

The results presented in Sect. 2.3 suggest that stratocumulus regions are particularly susceptible to such methodological errors, and particular care must be taken when studying such regions.

For large regions, spatial scale errors may lead to large errors in estimates of global cloud albedo effect radiative forcing. For regions on the scale of $60^\circ \times 60^\circ$, this study suggests that this methodological error in radiative forcing is of order 80%. The corresponding ocean-only error in radiative forcing is of order 70%.

This study focuses on the cloud properties, N_e and r_e, which are often of interest in cloud albedo effect studies. The methodological errors explored here highlight a potential source of inaccuracy in

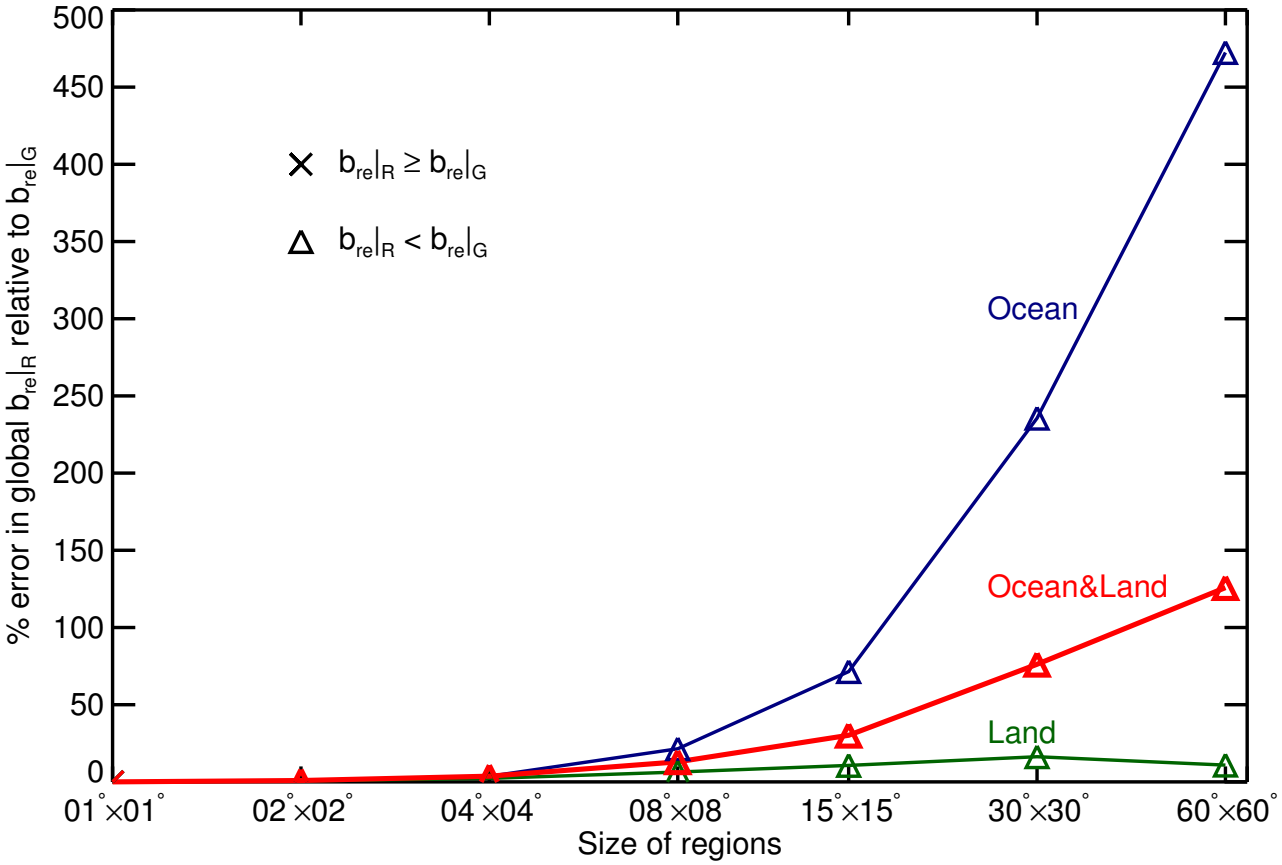

Figure 2.7: Same as Fig. 2.6, but for sensitivity of r_e to τ_a.

some of the cloud albedo effect studies mentioned in Sect. 2.1 [e.g Bréon et al., 2002, Kaufman et al., 2005, Bulgin et al., 2008, Quaas et al., 2008]. Although other cloud properties are not investigated here, it is likely that similar methodological errors may also affect the findings of studies which use large regions to investigate other aerosol indirect effects [e.g. Koren et al., 2005, 2008, Jones et al., 2009].

It is worth noting that even small regions experience changes in cloud regime and aerosol conditions, often as a result of meteorology. This may lead to spurious correlations unaccounted for in this study, and is the basis for future work.

2.4 Acknowledgements

The authors would like to thank Johannes Quaas, Till Wagner, Rosalind West, Andy Sayer, Gareth Thomas and Don Grainger for helpful discussions and comments on the manuscript. This research was conducted as part of a DPhil project funded by the UK Natural Environment Research Council.

Chapter 3

A storm-centric approach

When correlations between aerosol and cloud properties are observed, it is difficult to conclusively identify reasons for the observations. One possible way to investigate the importance of synoptic conditions would be to organise the data based on vertical motion or lower tropospheric stability. Another would be to classify the data according to cloud type, although the ISCCP classification scheme is not effective at distinguishing between low cloud classes, and different cloud types often occur together [Hahn et al., 2001]. In this chapter we begin exploring another two possibilities: classification according to storms (cyclones) and fronts.

3.1 Introduction

3.1.1 Aerosols, clouds, storms and fronts

It is possible that storms may lead to spurious correlations between aerosol and cloud properties. For example, the high windspeeds associated with storms may lead to high AODs, due to sea-salt over oceans and dust over continents. Since storms often produce high clouds with a high fractional coverage, this may contribute to observed negative CTP–AOD correlations and positive CF–AOD correlations (e.g. Figure 2.4 of Grandey [2009]; see also Sections 1.4.2 and 1.4.3 of the current report).

The frontal systems associated with extratropical cyclones often produce large bands of thick cloud. These clouds have the potential to both cycle and remove aerosol from the atmosphere. It would be interesting to investigate whether there are any significant differences between pre-frontal and post-frontal AOD. It is possible that such differences could contribute to spurious correlations between aerosol and cloud properties.

Although several studies have focused on the effect that climate change, including aerosol effects, may have on storms [e.g. Evan et al., 2008, Bengtsson et al., 2007b], comparatively little research has been done exploring the effect that storms may have on aerosols.

Over land, cold fronts have been observed to remove aerosols near the surface [e.g. Sheih et al., 1983, Jia et al., 2008]. However, the question remains as to how they affect the total aerosol column burden.

In a case study in West Africa, Crumeyrolle et al. [2008] investigate how a mesoscale convective system affects the properties of aerosol layers, through gust generation of dust aerosol, washout, cloud processing and the mixing of layers. During a cyclone over India, an increase in ground-level PM_{10}[1] was observed although the total AOD decreased, possibly due to winds leading to increased ventilation; over the Bay of Bengal, the aerosol load and dust increased, as did atmospheric water-vapour [Badarinath et al., 2008]. High windspeeds can lead to significantly increased AODs over

[1] Particulate matter with a diameter of less than 10 μm.

the ocean, due to both hygroscopic growth of aerosols and increased sea salt aerosol mass [Glantz et al., 2009]. Above a certain windspeed threshold, it is possible that sea salt concentrations near the surface may decrease due to scavenging by spray droplets [Pant et al., 2008], but it is unlikely that this decrease would be observed in column measurements of AOD.

Case studies are useful, but a statistical compositing approach should yield more robust and potentially more interesting results. As far as the author is aware, no previous research has considered this approach to investigating aerosol–cloud interactions.

3.1.2 Published storm-centric compositing studies

Several methods of compositing cyclones have been developed and used for meteorological research. Lau and Crane [1995] use ISCCP data to build composites of marine tropical and extratropical cyclones based on peaks in timeseries of cloud optical depth. Lau and Crane [1997] use the same method to compare surface observations to ISCCP. Norris and Iacobellis [2005] use a similar method, but choose warm and cold advection as the compositing variable. Minima in surface pressure can also be used to detect cyclone centres for compositing [Wang and Rogers, 2001]. Chang and Song [2006] build monthly cyclone composites of precipitation using ECMWF (European Centre for Medium-Range Weather Forecasts) ERA-40 reanalysis data, and then use satellite and surface observations for comparison. Field and Wood [2007] use NCEP-NCAR (National Centers for Environmental Prediction - National Center for Atmospheric Research) reanalysis surface pressure to locate the centres of approximately 1500 cyclones, and then build composites based on strength and moisture categories. Field et al. [2008] use the same compositing technique to compare output from different versions of the CAM (Community Atmosphere Model) GCM with satellite data.

A general feature detection and tracking method has been developed for cyclones [Hodges, 1994]. It uses relative vorticity, so can detect both tropical and extratropical cyclones. This method has been used successfully in a number of studies [e.g. Bengtsson et al., 2007a,b].

3.2 Method, data and properties used

3.2.1 Storm-tracking

Storms are tracked using Kevin Hodges' tracking code, known as TRACK [Hodges, 2008], which has been configured to track relative vorticity ω associated with extratropical cyclones in ECMWF operational analysis data. After removing tracks which persist for less than two days or move a distance of less than 1000 km, 1758 northern hemisphere probable extratropical cyclone tracks are found for the year 2007. For the remainder of this chapter, the tracked relative vorticity anomalies which remain following this filtering will be referred to as 'storms', regardless of whether they are actually extratropical cyclones.

Figure 3.1 shows one of the storm tracks detected by TRACK in some regridded ECMWF operational analysis relative vorticity data. This particular cyclone was detected in the north-eastern Atlantic Ocean and moved eastwards, as expected.

3.2.2 Satellite data

Aqua-MODIS joint cloud and aerosol irregularly gridded level 2 satellite data (MYDATML2, collection 5) are used. The cloud data are provided at ~ 5km$\times 5$km and the aerosol data at ~ 10km$\times 10$km resolution. Each data file covers a 'tile' of 5 minutes. The Scientific Data Sets (SDSs) currently used here are:

- Cloud_Optical_Thickness, τ_c, the cloud optical depth at 660 nm for all clouds (liquid and ice).

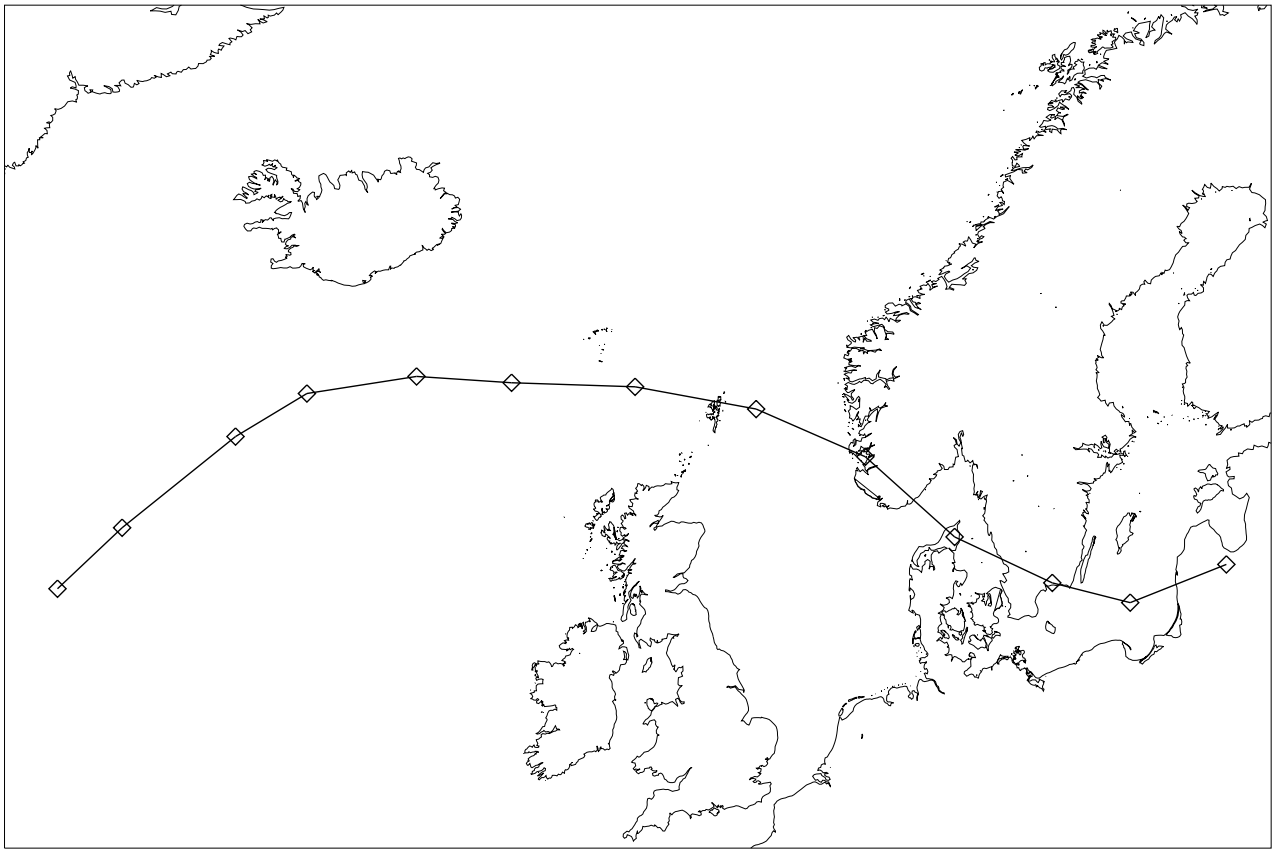

Figure 3.1: Example of an extratropical cyclone track identified by TRACK configuration. The track starts at the most westward lozenge at 1200 UTC on 2nd January 2007 and finishes at the most eastward lozenge at 1200 UTC on 5th January 2007. Each lozenge is separated by a time of 6 hours.

- Cloud_Top_Temperature, T_c, the temperature at the top of the cloud for all clouds.

One complete year (2007) of this data is used in the following analysis.

3.2.3 Storm-centric gridding and compositing

Using a cubic spline, the longitude, latitude and relative vorticity ω of each tracked storm are interpolated to match the overpass time for each 5 minute satellite tile. If part of the tile is displaced zonally and meridionally less than 2000 km from a storm centre, the tile and storm centre can be paired together.

Figures 3.2 and 3.3 show two examples of these storm–tile pairs. Visible cloud bands can be seen in Fig. 3.2(a), suggesting that the tracked storm does indeed appear to be an extratropical cyclone. The τ_c structure for this same storm, shown in Fig. 3.3(a), is also consistent with an extratropical cyclone with bands of thick cloud near the storm centre. However, the 'storm' in Figs. 3.2(b) and 3.3(b) appears to be an ω anomaly associated with a cold front, rather than the centre of an extratropical cyclone. The ω of (b) is much smaller than that of (a). Generally, higher ω values appear to be more likely to be extratropical cyclones. Further thresholding is being considered.

For each storm–tile pair, the irregularly gridded level 2 satellite data are re-gridded to a regular distance grid corresponding to zonal and meridional displacement from the storm centre. A resolution of 20km is used, being larger than the approximate resolution of the irregularly gridded input data and small enough potentially to see detailed structure in the cloud and aerosol fields. The size of the regridded plane is 4000 km $\times$ 4000 km, large enough to capture the large-scale structure of

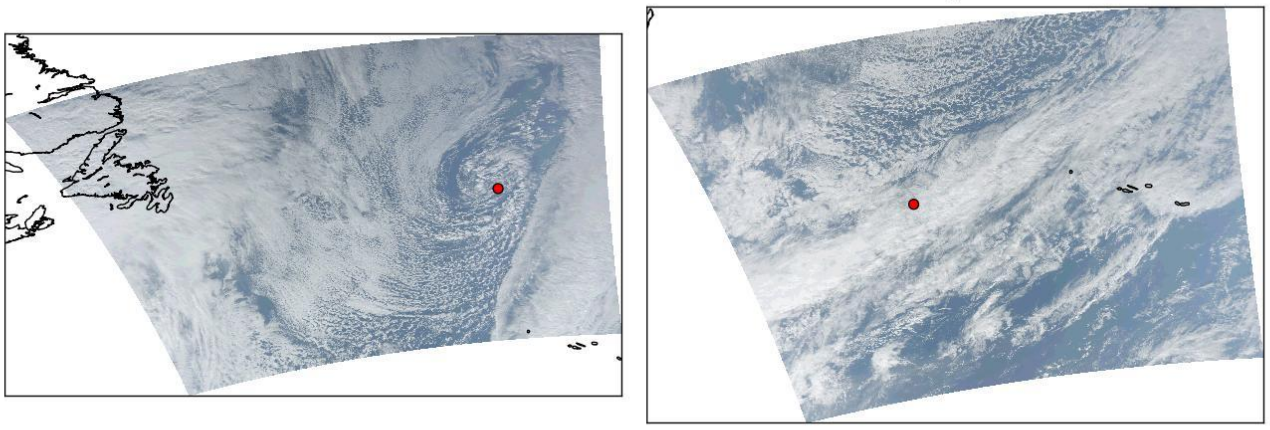

(a) RGB; 2007-01-02 15:45 UTC; relative vorticity $\omega = 6.89 \times 10^{-5}\text{s}^{-1}$

(b) RGB; 2007-01-04 15:30 UTC; $\omega = 1.27 \times 10^{-5}\text{s}^{-1}$

Figure 3.2: Pseudo-true colour red-green-blue (RGB) Aqua-MODIS images for two storm centres tracked by TRACK and interpolated to the time of the satellite data tile. The tracked storm centres are shown as red circles. Both are over the North Atlantic Ocean. The islands near the eastern edge of both maps are the Azores.

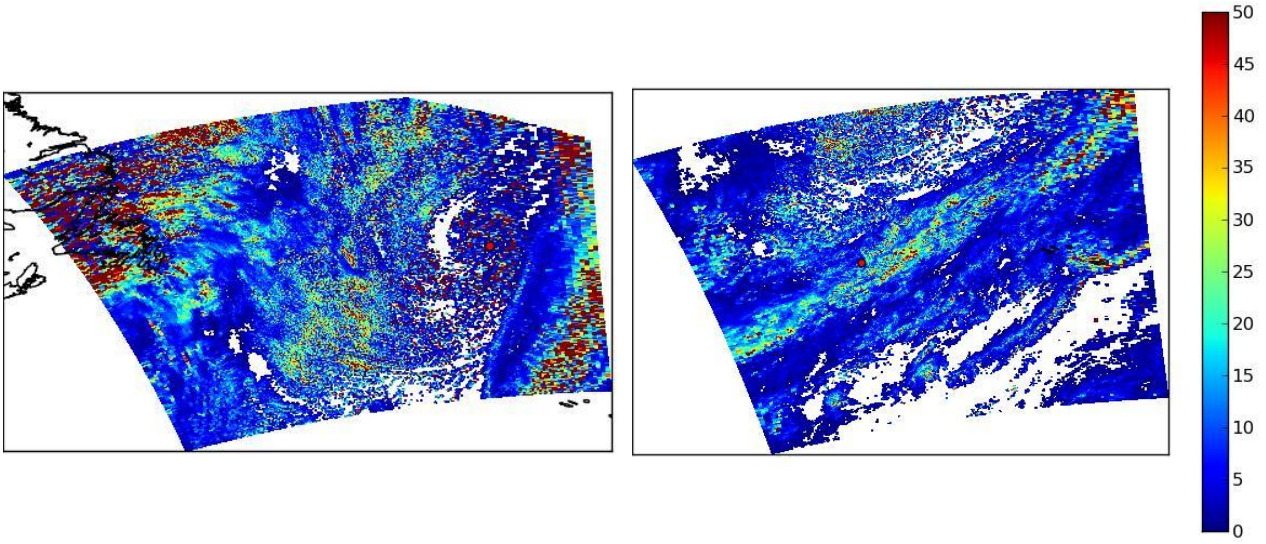

(a) τ_c; 2007-01-02 15:45 UTC

(b) τ_c; 2007-01-04 15:30 UTC

Figure 3.3: Aqua-MODIS retrieved cloud optical depth τ_c for the two storms shown in Fig. 3.2.

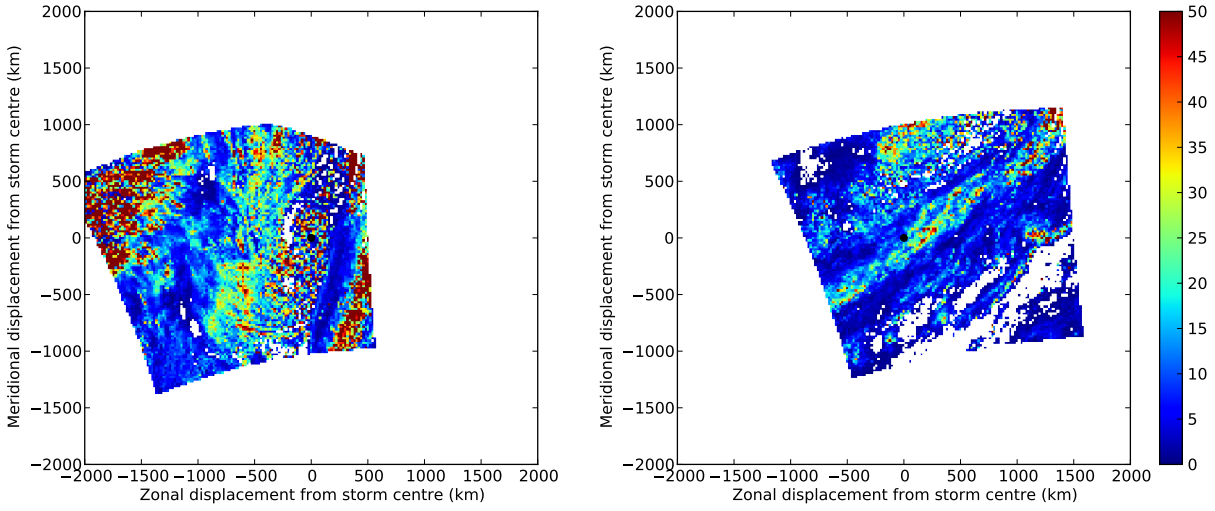

(a) τ_c; 2007-01-02 15:45 UTC

(b) τ_c; 2007-01-04 15:30 UTC

Figure 3.4: Storm-centric regularly gridded τ_c for the two storms shown in Figs. 3.2 and 3.3. The storm centres are at (0, 0), indicated by the black circle.

extratropical cyclones, with the storm at the centre of the plane. Over these scales, distortion due to neglecting the curvature of the earth is small. Figure 3.4 shows storm-centric regularly gridded τ_c data for the input τ_c data shown in Fig. 3.3.

After storm-centric regularly gridded data have been created for individual storms, these can be composited. The advantages of looking at a composite storm are that data coverage of the storm-centric domain will be increased significantly and that noise will be reduced, making some large-scale structure more evident than in individual cases. These composites suffer from the disadvantage that small-scale features, particularly those associated with specific storms, will be obscured. A composite storm is an average of many unique storms and does not necessarily represent a typical storm. However, although no individual storm may resemble the composite exactly, some of the large-scale features seen in a composite may often also be observed in individual storms.

Storm–tile pairs are separated into quartiles according to ω, with boundaries at 0.0, 3.1, 4.8, 6.5 and 14.0 $\times 10^{-5}\mathrm{s}^{-1}$. If all available Aqua-MODIS data for 2007 are included, each ω quartile contains ~ 1500 North-Atlantic storm–tile pairs, although only a small part of the storm-plane domain may overlap with many of the tiles. Comparing storm composites for the different ω quartiles allows the influence of storm-strength on large-scale structure to be investigated.

3.3 Preliminary results

Figure 3.5 shows τ_c composited according to ω, as outlined above. Blue areas represent comparatively thin cloud; green, yellow and red areas represent thicker clouds. As expected, an asymmetric thick cloud 'shield' can be seen near the centre of the composites. The thickness and size of this shield increases as the strength of the storm increases. This is consistent with Lau and Crane [1995], who used peaks in τ_c as the basis for storm detection in their compositing methodology.

Storm-centric composites of T_c are shown in Fig. 3.6. For weak storms, shown in Fig. 3.6(a), the dominant feature is a meridional gradient in T_c. As ω increases, the high cold top of the cloud 'shield' to the north and east of the storm centre becomes increasingly obvious. Figs. 3.6(c) and 3.6(d) display a very similar pattern to Fig. 3.7, the T_c composite of Field and Wood [2007].

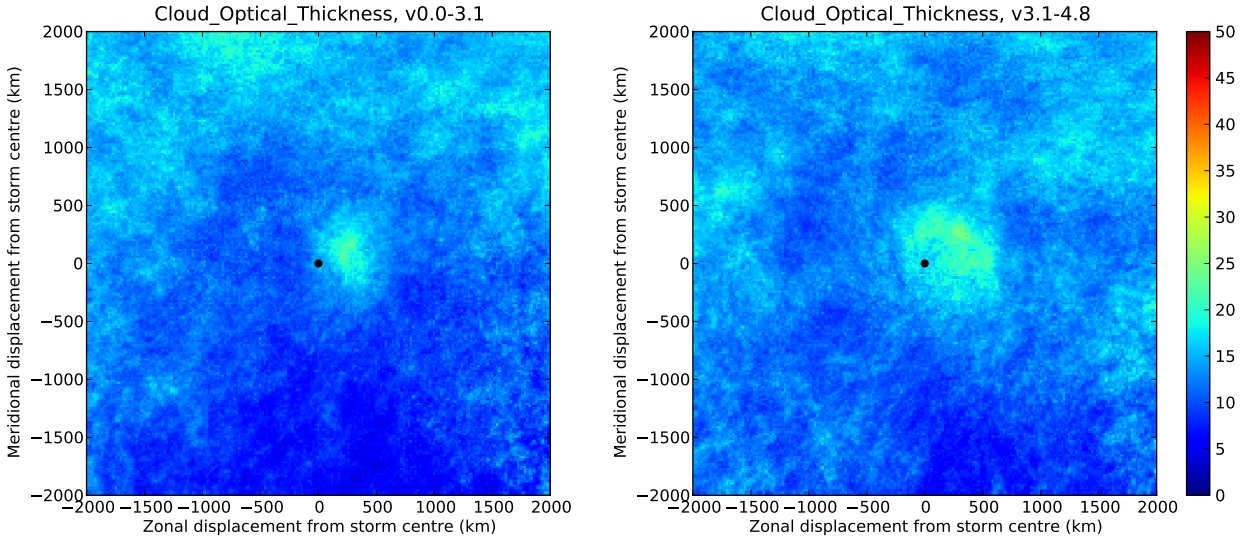

(a) τ_c; $0.0 \leq \omega < 3.1 \times 10^{-5}\mathrm{s}^{-1}$

(b) τ_c; $3.1 \leq \omega < 4.8 \times 10^{-5}\mathrm{s}^{-1}$

(c) τ_c; $4.8 \leq \omega < 6.5 \times 10^{-5}\mathrm{s}^{-1}$

(d) τ_c; $6.51 \leq \omega < 14.0 \times 10^{-5}\mathrm{s}^{-1}$

Figure 3.5: Storm-centric τ_c composited according to ω for all tracked North Atlantic storms in 2007.

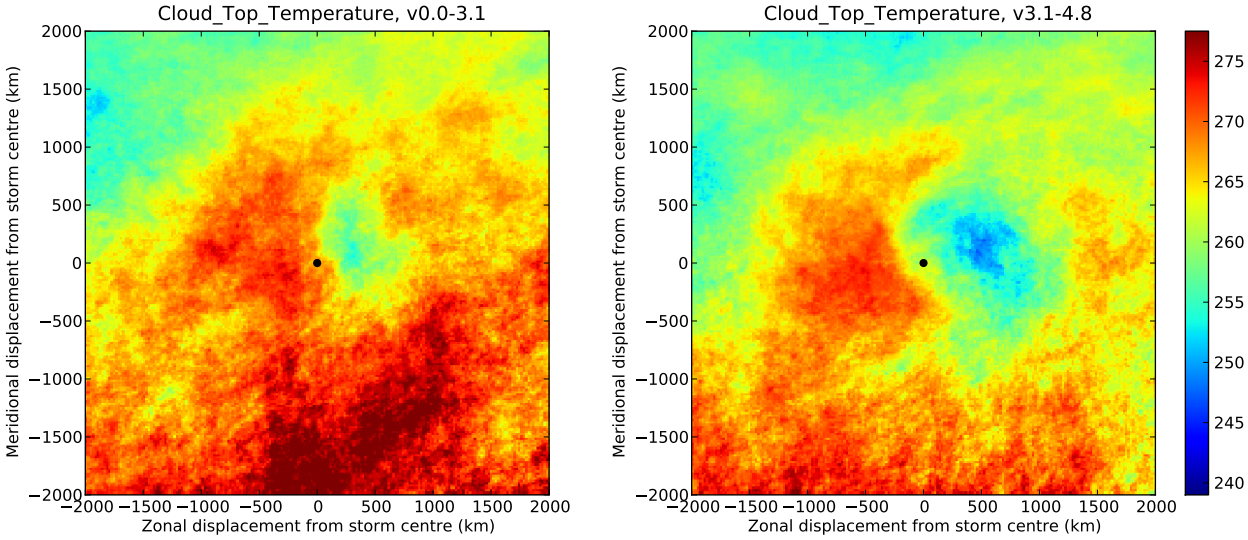

(a) T_c; $0.0 \leq \omega < 3.1 \times 10^{-5}\mathrm{s}^{-1}$

(b) T_c; $3.1 \leq \omega < 4.8 \times 10^{-5}\mathrm{s}^{-1}$

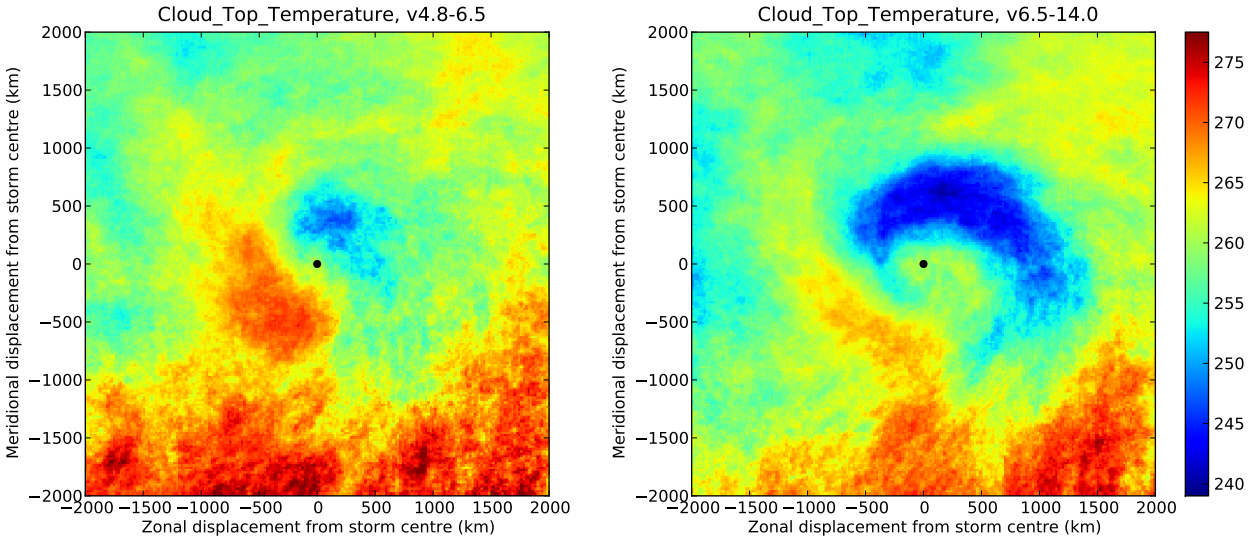

(c) T_c; $4.8 \leq \omega < 6.5 \times 10^{-5}\mathrm{s}^{-1}$

(d) T_c; $6.51 \leq \omega < 14.0 \times 10^{-5}\mathrm{s}^{-1}$

Figure 3.6: Same as Fig. 3.5, but for T_c.

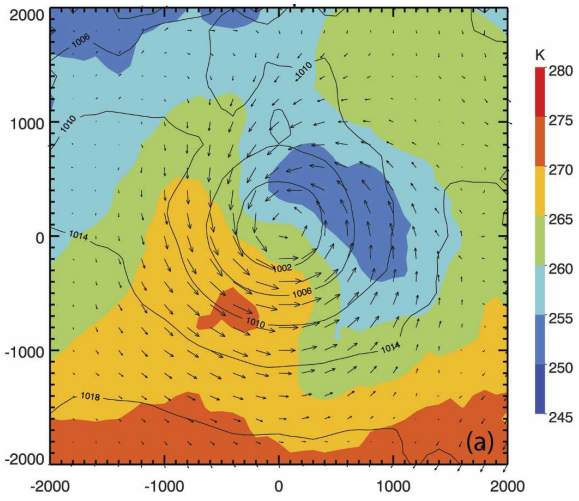

Figure 3.7: Mean T_c (colours), sea level pressure (black contours) and surface winds (arrows) for the North Atlantic composite cyclone of Field and Wood [2007]. [Figure taken from Field and Wood, 2007.]

3.4 Future work

3.4.1 Storms

The provisional results shown in Sect. 3.3 demonstrate that the compositing methodology of Sect. 3.2 yields τ_c and T_c composites consistent with previously published research. This methodology will be used to produce storm-centric composites of aerosol properties. Alongside MODIS satellite data, Global and regional Earth-system (Atmosphere) Monitoring using Satellite and in-situ data (GEMS) re-analysis aerosol forecast data will be used. If statistically robust patterns are observed, these will contibute to a discussion of the contibution of storm effects to observed aerosol–cloud relationships.

3.4.2 Fronts

Many attempts have been made to develop objective front identification methods [Hewson, 1998]. Objective front products are beginning to be used in scientific research [ECMWF, 2009]. It is possible that we may be able to obtain a license to use Met Office objective front code at some point in the future[2], in order look at aerosols on a pre-frontal and post-frontal basis. AERONET or CALIPSO data could be used to study how aerosol optical depth changes with the passage of fronts. Another possibility is that the positions of fronts could be taken into account when doing storm-centric gridding.

3.4.3 Anticyclones

As well as tracking cyclones (positive ω in the northern hemisphere), TRACK also offers the possibility of tracking anticyclones (negative ω in the northern hemisphere) [Hodges, 1994]. In order to investigate the effect of synoptic conditions on pollution, it should be possible to produce composites of aerosol and trace gas properties in an anticyclone-centric context.

[2]Personal correspondence with Tim Hewson (ECMWF) and Richard Swinbank (Met Office).

Chapter 4

Skills and future plans

4.1 Transferable skills

The author visited the Max Planck Institute for Meteorology (MPI-M; 5th October – 30th November 2009, Hamburg, Germany) as a guest of the International Max Planck Research School in Earth System Modelling (IMPRS-ESM). This was a productive visit to a highly stimulating interdisciplinary environment, providing an opportunity to work alongside some of the scientists based at MPI-M.

While at MPI-M, the author presented two talks. The author has also presented talks to the Climate Processes and EODG groups in AOPP, in addition to speaking at a student seminar and the annual AOPP retreat. The author attended and presented a poster at the European Space Agency Atmospheric Science Conference (7th–11th September 2009, Barcelona, Spain).

Writing and submitting a paper to *Atmospheric Chemistry and Physics* [Grandey and Stier, 2010] has provided an opportunity to practice written communication skills.

In addition to attending Oxford University Computing Services courses on InDesign and Illustrator, the author has continued to develop and consolidate computing skills concerning the use of Linux systems, Mac OSX, LaTeX, InkScape, Microsoft PowerPoint, IDL, Python and Bash.

4.2 Thesis outline

4.2.1 Chapter 1: Introduction

Chapter 1 will provide an introduction to aerosols, clouds and climate, including a literature review. The aims of the project will be outlined.

4.2.2 Chapter 2: Satellites and observational methods

Chapter 2 will introduce the satellites and observational datasets of interest to the research.

4.2.3 Chapter 3: Models

Chapter 3 will introduce any general circulation models (GCMs) relevant to the research. GCMs will be used in Chapters 5 and 7.

4.2.4 Chapter 4: Spatial scale considerations for aerosol indirect effect studies

Chapter 4 will discuss the importance of spatial scale considerations with respect to indirect effect studies, following Grandey and Stier [2010].

4.2.5 Chapter 5: An intercomparison of aerosol–cloud interactions in models and satellite data

Taking into account the results of Chapter 4, and building on the work of Quaas et al. [2009], spatial distributions of aerosol–cloud relationships in different GCMs and satellite datasets will be compared.

4.2.6 Chapter 6: Storm-centric analysis of satellite aerosol datasets

Chapter 6 will present results from investigating aerosols and clouds using a storm-centric approach.

4.2.7 Chapter 7: Storm-centric analysis of a GCM

Depending on the findings of Chapter 6, some of the storm-centric analyses may be extended to investigate output from GCMs. GCMs allow different processes, such as aerosol–cloud microphysics, to be turned on or off, thus allowing hypotheses to be tested. These results will be presented in Chapter 7.

4.2.8 Chapter 8: Conclusion

The main findings will be discussed and summarised in Chapter 8.

4.3 Timetable

4.3.1 Summer 2010

- Submit second year report and have viva.
- Respond to referee comments on Grandey and Stier [2010].
- Present poster comparing aerosol–cloud relationships in GCM and satellite data at the AeroCom Workshop (27^{th}–30^{th} September, Oxford).
- Present talk at AOPP Annual Retreat (30^{th} September – 1^{st} October).

4.3.2 Michaelmas Term 2010

- Complete development of tools for intercomparison of aerosol–cloud relationships in satellite and GCM data (Chapter 5).
- Complete storm-centric satellite analysis (Chapter 6).
- Present poster on storm-centric analysis at the AGU Fall Meeting (13^{th}–17^{th} December, San Francisco, California, USA).
- Finish draft of Chapter 4.

4.3.3 Hilary Term 2011

- Complete storm-centric model analysis (Chapter 7).
- Finish draft of Chapters 2 and 6.

	2010		2011		
	Summer	MT	HT	TT	Summer
Chapter 1					W
Chapter 2			W		
Chapter 3				W	
Chapter 4		W			
Chapter 5	R	R		W	
Chapter 6	R	R	W		
Chapter 7			R	W	
Chapter 8					W

Table 4.1: Timetable for research (R) and writing (W) of thesis chapters.

4.3.4 Trinity Term 2011

- Finish drafts of Chapters 3, 5 and 7.

4.3.5 Summer 2011

- Finish drafts of Chapters 1 and 8.
- Submit thesis at the end of September 2011.

Bibliography

A. S. Ackerman, O. B. Toon, D. E. Stevens, A. J. Heymsfield, V. Ramanathan, and E. J. Welton. Reduction of tropical cloudiness by soot. *Science*, 288(5468):1042–1047, 2000. doi: 10.1126/science.288.5468.1042.

B. A. Albrecht. Aerosols, Cloud Microphysics, and Fractional Cloudiness. *Science*, 245(4923): 1227–1230, 1989.

O. Altaratz, I. Koren, and T. Reisin. Humidity impact on the aerosol effect in warm cumulus clouds. *Geophys. Res. Lett.*, 35:L17804, 2008. doi: 10.1029/2008GL034178.

M. O. Andreae. Correlation between cloud condensation nuclei concentration and aerosol optical thickness in remote and polluted regions. *Atmos. Chem. Phys.*, 9:543–556, 2009.

M. O. Andreae, D. Rosenfeld, P. Artaxo, A. A. Costa, G. P. Frank, K. M. Longo, and M. A. F. Silva-Dias. Smoking Rain Clouds over the Amazon. *Science*, 303(5662):1337–1342, 2004.

M. O. Andreae, C. D. Jones, and P. M. Cox. Strong present-day aerosol cooling implies a hot future. *Nature*, 435:1187–1190, 2005. doi: 10.1038/nature03671.

M. Andrejczuk, J. M. Reisner, B. Henson, M. K. Dubey, and C. A. Jeffery. The potential impacts of pollution on a nondrizzling stratus deck: Does aerosol number matter more than type? *J. Geophys. Res.*, page D19204, 2008. doi: 10.1029/2007JD009445.

A. Arakawa. The cumulus parameterization problem: Past, present, and future. *J. Climate*, 17(13): 2493–2525, 2004.

K. V. S. Badarinath, S. K. Kharol, V. Krishna Prasad, D. G. Kaskaoutis, and H. D. Kambezidis. Variation in aerosol properties over Hyderabad, India during intense cyclonic conditions. *Int. J. Remote Sens.*, 29(15):4575–4597, 2008. doi: 10.1080/01431160801950170.

W. L. Barnes, T. S. Pagano, and V. V. Salomonson. Prelaunch characteristics of the moderate resolution imaging spectroradiometer (MODIS) on EOS-AMI. *IEEE T. Geosci. Remote*, 36(4):1088–1100, 1998.

M. L. Bell, J. M. Samet, and F. Dominici. Time-series studies of particulate matter. *Annu. Rev. Publ. Health*, 25:247–280, 2004. doi: 10.1146/annurev.publhealth.25.102802.124329.

L. Bengtsson, K. I. Hodges, and M. Esch. Tropical cyclones in a T159 resolution global climate model: comparison with observations and re-analyses. *Tellus*, 59 A(4), 2007a. doi: 10.111/j.1600-0870.2007.00236.x.

L. Bengtsson, K. I. Hodges, M. Esch, N. Keenlyside, L. Kornblueh, L. Jing-Jia, and T. Yamagata. How may tropical cyclones change in a warmer climate? *Tellus*, 59 A(4), 2007b. doi: 10.111/j.1600-0870.2007.00251.x.

S. Bony and J.-L. Dufresne. Marine boundary layer clouds at the heart of tropical cloud feedback uncertainties in climate models. *Geophys. Res. Lett.*, 32, 2005. doi: 10.1029/2005GL023851.

S. Bony, R. Colman, V. M. Kattsov, R. P. Allan, C. S. Bretherton, J.-L. Dufresne, A. Hall, S. Hallegatte, M. M. Holland, W. Ingram, D. A. Randall, B. J. Soden, G. Tselioudis, and M. J. Webb. How Well Do We Understand and Evaluate Climate Change Feedback Processes? *J. Climate*, 19: 3445–3482, 2006.

J.-L. Brenguier, H. Pawlowska, L. Schüller, R. Preusker, J. Fischer, and Y. Fouquart. Radiative properties of boundary layer clouds: Droplet effective radius versus number concentration. *J. Atmos. Sci.*, 57(6):803–821, 2000.

J. I. Brennan, Y. J. Kaufman, I. Koren, and R. R. Li. Aerosol–Cloud Interaction—Misclassification of MODIS Clouds in Heavy Aerosol. *IEEE T. Geosci. Remote*, 43(4):911–915, 2005. doi: 10.1109/TGRS.2005.844662.

F.-M. Bréon and M. Doutriaux-Boucher. A Comparison of Cloud Droplet Radii Measured From Space. *IEEE T. Geosci. Remote*, 43(8):1796–1805, 2005. doi: 10.1109/TGRS.2005.852838.

F.-M. Bréon, Tanré. D., and S. Generoso. Aerosol Effect on Cloud Droplet Size Monitored from Satellite. *Science*, 295:834–838, 2002. doi: 10.1126/science.1066434.

C. E. Bulgin, P. I. Palmer, G. E. Thomas, C. P. G. Arnold, E. Campmany, E. Carboni, R. G. Grainger, C. Poulsen, R. Siddans, and B. N. Lawrence. Regional and seasonal variations of the Twomey indirect effect as observed by the ATSR-2 satellite instrument. *Geophys. Res. Lett.*, 35(2):L02811, 2008. doi: 10.1029/2007GL031394.

E. K. M. Chang and S. Song. The Seasonal Cycles in the Distribution and Precipitation around Cyclones in the Western North Pacific and Atlantic. *J. Atmos. Sci.*, 63:815–839, 2006.

Y.-S. Choi, C.-H. Ho, H.-R. Oh, R. J. Park, and C.-G. Song. Estimating bulk optical properties of aerosols over the western North Pacific by using MODIS and CERES measurements. *Atmos Environ*, 43:5654–5660, 2009. doi: 10.1016/j.atmosenv.2009.07.036.

CNES. CALIPSO: Mission studying the atmosphere, 2009a. `http://smsc.cnes.fr/CALIPSO/` [Accessed 24th August 2009].

CNES. PARASOL: Mission studying the atmosphere, 2009b. `http://smsc.cnes.fr/PARASOL/` [Accessed 22nd August 2009].

CNES. POLDER: Atmosphere, Land and Ocean mission, 2009c. `http://smsc.cnes.fr/POLDER/` [Accessed 22nd August 2009].

Colorado State University. CLOUDSAT, 2009. `http://eospso.gsfc.nasa.gov/` [Accessed 22nd August 2009].

S. Crumeyrolle, L. Gomes, P. Tulet, A. Matsuki, A. Schwarzenboeck, and K. Crahan. Increase of the aerosol hygroscopicity by cloud processing in a mesoscale convective system: a case study from the AMMA campaign. *Atmos. Chem. Phys.*, 8:6907–6924, 2008.

Z. Cui, K. S. Carslaw, Y. Yin, and S. Davies. A numerical study of aerosol effects on the dynamics and microphysics of a deep convective cloud in a continental environment. *J. Geophys. Res.*, 111, 2006. doi: 10.1029/2005JD005981.

K. L. Denman, G. Brasseur, A. Chidthaisong, P. Ciais, P. M. Cox, R. E. Dickinson, D. Hauglustaine, E. Heinze, C. Holland, D. Jacob, U. Lohmann, S. Ramachandran, P. L. da Silva Dias, S. C. Wofsy, and X. Zhang. *Couplings Between Changes in the Climate System and Biogeochemistry. In: Climate Change 2007: The Physical Science Basis. Contribution of Working Group 1 to the Fourth Assessment Report of the Intergovernmental Panel on Climate Change*. Cambridge University Press, 2007.

P.-Y. Deschamps, F.-M. Breon, M. Leroy, A. Podaire, A. Bricaud, J.-C. Buriez, and G. Seze. POLDER mission: instrument characteristics and scientific objectives. *IEEE T. Geosci. Remote*, 32(3):598–614, 1994. doi: 10.1109/36.297978.

D. J. Diner, J. C. Beckert, T. H. Reilly, C. J. Bruegge, J. E. Conel, R. A. Kahn, J. V. Martonchik, T. P. Ackerman, R. Davies, S. A. W. Gerstl, H. R. Gordon, J.-P. Muller, R. B. Myneni, P. J. Sellers, B. Pinty, and M. M. Verstraete. Multi-angle imaging spectroradiometer (MISR) instrument description and experiment overview. *IEEE T. Geosci. Remote*, 36(4):1072–1087, 1998.

ECMWF. T-PARC - THORPEX Pacific Asian Regional Campaign, 2009. `http://www.ecmwf.int/research/WMO_projects/TPARC` [Accessed 20th August 2009].

ESA. Envisat ESA Mission, 2009. `http://envisat.esa.int/` [Accessed 24th August 2009].

W. E. Esaias, M. R. Abbott, I. Barton, O. B. Brown, J. W. Campbell, K. L. Carder, D. K. Clark, R. H. Evans, F. E. Hoge, H. R. Gordon, W. M. Balch, R. Letelier, and P. J. Minnett. An overview of MODIS capabilities for ocean science observations. *IEEE T. Geosci. Remote*, 36(4):1250–1265, 1998.

A. T. Evan, A. K. Heidinger, R. Bennartz, V. Bennington, H. Mahowald, N. M. amd Corrada-Bravo, C. S. Velden, G. Myhre, and J. P. Kossin. Ocean temperature forcing by aerosols across the Atlantic tropical cyclone development region. *Geochem. Geophy. Geosy.*, 9(5):Q05V04, 2008. doi: 10.1029/2007GC001774.

G. Feingold, L. A. Remer, J. Ramaprasad, and Y. J. Kaufman. Analysis of smoke impact on clouds in Brazilian biomass burning regions: An extension of Twomey's approach. *J. Geophys. Res.*, 106: 22,907–22,922, 2001. doi: 10.1029/2001JD000732.

R. P. Feynman. *The Character of the Physical Law*. Penguin, 2007.

P. R. Field and R. Wood. Precipitation and Cloud Structure in Midlatitude Cyclones. *J. Climate*, 20 (2):233–254, 2007.

P. R. Field, A. Gettelman, R. B. Neale, R. Wood, P. J. Rasch, and H. Morrison. Midlatitude Cyclone Compositing to Constrain Climate Model Behaviour Using Satellite Observations. *J. Climate*, 21: 5887–5903, 2008. doi: 10.1175/2008JCLI2235.1.

P. Forster, V. Ramaswamy, P. Artaxo, T. Berntsen, R. Betts, D. W. Fahey, J. Haywood, J. Lean, D. C. Lowe, G. Myhre, J. Nganga, R. Prinn, G. Raga, M Schultz, and R. Van Dorland. *Changes in Atmospheric Constituents and in Radiative Forcing. In: Climate Change 2007: The Physical Science Basis. Contribution of Working Group 1 to the Fourth Assessment Report of the Intergovernmental Panel on Climate Change*. Cambridge University Press, 2007.

R. C. George and R. Wood. Subseasonal variability of low cloud radiative properties of the southeast Pacific Ocean. *Atmos. Chem. Phys.*, 10:4047–4063, 2010.

P. Glantz, E. D. Nilsson, and W. von Hoyningen-Huene. Estimating a relationship between aerosol optical thickness and surface wind speed over the ocean. *Atmos. Res.*, 92:58–68, 2009. doi: 10.1016/j.atmosres.2008.08.010.

B. S. Grandey. Investigating aerosol–cloud interactions (First year report). University of Oxford, 45pp., 2009.

B. S. Grandey and P. Stier. A critical look at spatial scale choices in satellite-based aerosol indirect effect studies. *Atmos. Chem. Phys. Discuss.*, 10:15417–15440, 2010. doi: 10.5194/acpd-10-15417-2010.

P. Grennfelt and Ø. Hov. Regional air pollution at a turning point. *Ambio*, 34(1):2–10, 2005.

C. J. Hahn, W. B. Rossow, and S. G. Warren. ISCCP Cloud Properties Associated with Standard Cloud Types Identified in Individual Surface Observations. *J. Climate*, 14:11–28, 2001.

J. Haywood and O. Boucher. Estimates of the direct and indirect radiative forcing due to tropospheric aerosols: A review. *Rev. Geophys.*, 38(4):513–543, 2000. doi: 10.1029/1999RG000078.

J. M. Haywood and K. P. Shine. The effect of anthropogenic sulfate and soot aerosol on the clear sky planetary radiation budget. *Geophys. Res. Lett.*, 22(5):603–606, 1995.

T. D. Hewson. Objective fronts. *Meteorol. Appl.*, 5:37–65, 1998.

K. I. Hodges. A General Method for Tracking Analysis and Its Application to Meteorological Data. *Mon. Weather Rev.*, 122:2573–2586, 1994.

K. I. Hodges. TRACK, 2008. `http://www.nerc-essc.ac.uk/~kih/TRACK/Track.html` [Accessed 21st August 2009].

B. N. Holben, T. F. Eck, I. Slutsker, D. Tanré, J. P. Buis, A. Setzer, E. Vermote, J. A. Reagan, Y. J. Kaufman, T. Nakajima, F. Lavenu, I. Jankowiak, and A. Smirnov. AERONET - A federated instrument network and data archive for aerosol characterization. *Remote Sens. Environ.*, 66(1): 1–16, 1998. doi: 10.1016/S0034-4257(98)00031-5.

A. Huete, K. Didan, T. Miura, E. P. Rodriguez, X. Gao, and L. G. Ferreira. Overview of the radiometric and biophysical performance of the MODIS vegetation indices. *Remote Sens. Environ.*, 83 (1-2):195–213, 2002. doi: 10.1016/S0034-4257(02)00096-2.

M. Z. Jacobson. *Fundamentals of Atmospheric Modeling, Second Edition*. Cambridge University Press, 2005.

M.-J. Jeong and N. C. Hsu. Retrievals of aerosol single-scattering albedo and effective aerosol layer height for biomass-burning smoke: Synergy derived from "A-Train" sensors. *Geophys. Res. Lett.*, 35(24):L24801, 2008. doi: 10.1029/2008GL036279.

Y. Jia, K. A. Rahn, K. He, T. Wen, and Y. Wang. A novel technique for quanifying the regional component of urban aerosol solely from its sawtooth cycles. *J. Geophys. Res.*, 113:D21309, 2008. doi: 10.1029/2008JD010389.

H. Jiang, H. Xue, A. Teller, G. Feingold, and Z. Levin. Aerosol effects on the lifetime of shallow cumulus. *Geophys. Res. Lett.*, 33, 2006. doi: 10.1029/2006GL026024.

T. A. Jones, S. A. Christopher, and J. Quaas. A six year satellite-based assessment of the regional variations in aerosol indirect effects. *Atmos. Chem. Phys.*, 9:4091–4114, 2009.

Y. J. Kaufman, D. D. Herring, K. J. Ranson, and J. G. Collatz. Earth observing system AMI mission to earth. *IEEE T. Geosci. Remote*, 36(4):1045–1055, 1998.

Y. J. Kaufman, I. Koren, L. A. Remer, D. Rosenfeld, and Y. Rudich. The effect of smoke, dust, and pollution aerosol on shallow cloud development over the Atlantic Ocean. *P. Natl. Acad. Sci. USA*, 102(32):11207–11212, 2005. doi: 10.1073/pnas.0505191102.

I. M. Kennedy. The health effects of combustion-generated aerosols. *P. Combust. Inst.*, 31 II:2757–2770, 2007. doi: 10.1016/j.proci.2006.08.116.

A. Khain, D. Rosenfeld, and A. Pokrovsky. Aerosol impact on the dynamics and microphysics of deep convective clouds. *Q. J. Roy. Meteor. Soc.*, 131:2639–2663, 2005. doi: 10.1256/qj.04.62.

J. T. Kiehl. Twentieth century climate model response and climate sensitivity. *Geophys. Res. Lett.*, 34(22):L22710, 2007. doi: 10.1029/2007GL031383.

V. R. Kiran, M. Rajeevan, S. V. B. Rao, and N. P. Rao. Analysis of variations of cloud and aerosol properties associated with active and break spells of Indian summer monsoon using MODIS data. *Geophys. Res. Lett.*, 36:L09706, 2009. doi: 10.1029/2008GL037135.

I. Koren, Y. J. Kaufman, D. Rosenfeld, L. A. Remer, and Y. Rudich. Aerosol invigoration and restructuring of the Atlantic convective clouds. *Geophys. Res. Lett.*, 32(14), 2005. doi: 10.1029/2005GL023187.

I. Koren, L. A. Remer, Y. J. Kaufman, Y. Rudich, and J. V. Martins. On the twilight zone between clouds and aerosols. *Geophys. Res. Lett.*, 34, 2007. doi: 10.1029/2007GL029253.

I. Koren, J. V. Martins, L. A. Remer, and H. Afargan. Smoke Invigorations Versus Inhibition of Clouds over the Amazon. *Science*, 321:946–949, 2008. doi: 10.1126/science.1159185.

T. L. Kubar, D. L. Hartmann, and R. Wood. Understanding the Importance of Microphysics and Macrophysics for Warm rain in Marine Low Clouds. Part I: Satellite Observations. *J. Atmos. Sci.*, 66:2953–2972, 2009. doi: 10.1175/2009JAS3071.1.

S. J. Lambert and G. J. Boer. CMIP1 evaluation and intercomparison of coupled climate models. *Clim. Dynam.*, 17:83–106, 2001.

N.-C. Lau and M. W. Crane. A Satellite View of the Synoptic-Scale Organization of Cloud Properties in Midlatitude and Tropical Circulation Systems. *Mon. Weather Rev.*, 123:1984–2006, 1995.

N.-C. Lau and M. W. Crane. Comparing Satellite and Surface Observations of Cloud Patterns in Synoptic-Scale Circulation Systems. *Mon. Weather Rev.*, 125:3172–3189, 1997.

T. S. L'Ecuyer, W. Berg, J. Haynes, M. Lebsock, and T. Takemura. Global observations of aerosol impacts on precipitation occurrence in warm maritime clouds. *J. Geophys. Res.*, 114:D09211, 2009. doi: 10.1029/2008JD011273.

F. Li and V. Ramanathan. Winter to summer monsoon variation of aerosol optical depth over the tropical Indian Ocean. *J. Geophys. Res.*, 107, 2002. doi: 10.1029/2001JD000949.

J. C. Liu, C. Schaaf, A. Strahler, Z. T. Jiao, Y. M. Shuai, Q. L. Zhang, M. Roman, J. A. Augustine, and E. G. Dutton. Validation of Moderate Resolution Imaging Spectroradiometer (MODIS) albedo retrieval algorithm: Dependence of albedo on solar zenith angle. *J. Geophys. Res.*, page D01106, 2009. doi: 10.1029/2008JD009969.

U. Lohmann. A glaciation indirect aerosol effect caused by soot aerosols. *Geophys. Res. Lett.*, 29 (4), 2002. doi: 10.1029/2001GL014357.

U. Lohmann and J. Feichter. Global indirect aerosol effects: a review. *Atmos. Chem. Phys.*, 5: 715–737, 2005.

U. Lohmann, I. Koren, and Y. J. Kaufman. Disentangling the role of microphysical and dynamical effects in determining cloud properties over the Atlantic. *Geophys. Res. Lett.*, 33, 2006. doi: 10.1029/2005GL024625.

A. Marshak, S. Platnick, T. Várnai, G. Wen, and R. F. Cahalan. Impact of three-dimensional radiative effects on satellite retrievals of cloud droplet sizes. *J. Geophys. Res.*, 111:D09207, 2006. doi: 10.1029/2005JD006686.

A. McComiskey, G. Feingold, A. S. Frisch, D. D. Turner, M. A. Miller, J. C. Chiu, Q. Min, and J. A. Ogren. An assessment of aerosol-cloud interactions in marine stratus clouds based on surface remote sensing. *J. Geophys. Res.*, 114:D09203, 2009. doi: 10.1029/2008JD011006.

G. A. Meehl, T. F. Stocker, W. D. Collins, P. Friedlingstein, A. T. Gaye, J. M. Gregory, A. Kitoh, R. Knutti, J. M. Murphy, A. Noda, S. C. B. Raper, I. G. Watterson, A. J. Weaver, and Z.-C. Zhao. *Global Climate Projections. In: Climate Change 2007: The Physical Science Basis. Contribution of Working Group 1 to the Fourth Assessment Report of the Intergovernmental Panel on Climate Change*. Cambridge University Press, 2007.

S. Menon, A. D. Del Genio, Y. Kaufman, R. Bennartz, D. Koch, N. Loeb, and D. Orlikowski. Analyzing signatures of aerosol-cloud interactions from satellite retrievals and the GISS GCM to constrain the aerosol indirect effect. *J. Geophys. Res.*, 113, 2008. doi: 10.1029/2007JD009442.

N. Meskhidze, L. A. Remer, S. Platnick, R. Negrón Juárez, A. M. Lichtenberger, and A. R. Aiyyer. Exploring the differences in cloud properties observed by the Terra and Aqua MODIS sensors. *Atmos. Chem. Phys.*, 9:3461–3475, 2009.

C. T. Mutlow. The ATSR instrument. *Earth Observation Quarterly*, 40:14–15, 1993.

T. Nakajima and M. D. King. Determination of the Optical Thickness and Effective Particle Radius of Clouds from Reflected Solar Radiation Measurements. Part I: Theory. *J. Atmos. Sci.*, 47(15): 1878–1893, 1990.

NASA. The Cloud-Aerosol Lidar and Infrared Pathfinder Satellite Observation (CALIPSO), 2009a. `http://www-calipso.larc.nasa.gov/` [Accessed 24th August 2009].

NASA. NASA Earth Observatory, 2010. `http://earthobservatory.nasa.gov/` [Accessed 18th August 2010].

NASA. The Earth Observing System Project Science Office, 2009b. `http://eospso.gsfc.nasa.gov/` [Accessed 22nd August 2009].

NASA. LAADS Web: Level 1 and Atmosphere Archive Distribution System, 2009c. `http://ladsweb.nascom.nasa.gov/index.html` [Accessed 21st August 2009].

NASA. MISR: Multi-angle Imaging SpectroRadiometer, 2009d. `http://www-misr.jpl.nasa.gov/index.html` [Accessed 21st August 2009].

NASA. MODIS Atmosphere, 2009e. `http://modis-atmos.gsfc.nasa.gov/index.html` [Accessed 21st August 2009].

NASA. MODIS Web, 2009f. http://modis.gsfc.nasa.gov/ [Accessed 21st August 2009].

F. J. Nober, H. F. Graf, and D. Rosenfeld. Sensitivity of the global circulation to the suppression of precipitation by anthropogenic aerosols. *Global Planet. Change*, 37:57–80, 2003.

J. R. Norris and S. F. Iacobellis. North Pacific Cloud Feedbacks Inferred from Synoptic-Scale Dynamic and Thermodynamic Relationships. *J. Climate*, 18:4862–4878, 2005.

V. Pant, C. G. Deshpande, and A. K. Kamra. On the aerosol number concentration–wind speed relationship during a severe cyclonic storm over south Indian Ocean. *J. Geophys. Res.*, 113:D02206, 2008. doi: 10.1029/2006JD008035.

C. L. Parkinson. Aqua: An Earth-Observing Satellite Mission to Examin Water and Other Climate Variables. *IEEE T. Geosci. Remote*, 41(2):173–183, 2003. doi: 10.1109/TGRS.2002.808319.

J. E. Penner, J. Quaas, T. Storelvmo, T. Takemura, O. Boucher, H. Guo, A. Kirkevåg, J. E. Kristjánsson, and Ø. Seland. Model intercomparison of indirect aerosol effects. *Atmos. Chem. Phys.*, 6(11):3391–3405, 2006.

C. Piani, D. J. Frame, D. A. Stainforth, and M. R. Allen. Constraints on climate change from a multi-thousand member ensemble of simulations. *Geophys. Res. Lett.*, 32(23):1–5, 2005. doi: 10.1029/2005GL024452.

R. Pincus and M. B. Baker. Effect of precipitation on the albedo susceptibility of clouds in the marine boundary layer. *Nature*, 372(6503):250–252, 1994.

D. J. Posselt, G. L. Stephens, and M. Miller. CLOUDSAT: Adding a New Dimension to a Classical View of Extratropical Cyclones. *B. Am. Meteorol. Soc.*, 89(5):599–609, 2008.

J. Quaas, O. Boucher, and U. Lohmann. Constraining the total aerosol indirect effect in the LMDZ and ECHAM4 GCMs using MODIS satellite data. *Atmos. Chem. Phys.*, 6(4):947–955, 2006.

J. Quaas, O. Boucher, N. Bellouin, and S. Kinne. Satellite-based estimate of the direct and indirect aerosol climate forcing. *J. Geophys. Res.*, 113, 2008. doi: 10.1029/2007JD008962.

J. Quaas, Y. Ming, S. Menon, T. Takemura, M. Wang, J. E. Penner, A. Gettelman, U. Lohmann, N. Bellouin, O. Boucher, A. Sayer, G. E. Thomas, A. McComiskey, G. Feingold, C. Hoose, J. E. Kristjánsson, X. Liu, Y. Balkanski, L. J. Donner, P. A. Ginoux, P. Stier, B. Grandey, J. Feichter, I. Sednev, S. E. Bauer, D. Koch, R. G. Grainger, A. Kirkevåg, T. Iversen, Ø Seland, R. Easter, S. J. Ghan, P. J. Rasch, H. Morrison, J.-F. Lamarque, M. J. Iacono, S. Kinne, and M. Schulz. Aerosol indirect effects – general circulation model intercomparison and evaluation with satellite data. *Atmos. Chem. Phys.*, 9:8697–8717, 2009.

J. Quaas, B. Stevens, P. Stier, and U. Lohmann. Interpreting the cloud cover aerosol optical depth relationship found in satellite data using a general circulation model. *Atmospheric Chemistry and Physics*, 10(13):6129–6135, 2010. doi: 10.5194/acp-10-6129-2010. URL http://www.atmos-chem-phys.net/10/6129/2010/.

RAL. The ATSR Project, 2003. http://www.atsr.rl.ac.uk/ [Accessed 21st August 2009].

D. A. Randall, R. A. Wood, S. Bony, R. Colman, T. Fichefet, J. Fyfe, V. Kattsov, A. Pitman, J. Shukla, J. Srinivasan, R. J. Stouffer, A. Sumi, and K. E. Taylor. *Climate Models and Their Evaluation. In: Climate Change 2007: The Physical Science Basis. Contribution of Working Group 1 to the Fourth Assessment Report of the Intergovernmental Panel on Climate Change*. Cambridge University Press, 2007.

J. Redemann, Q. Zhang, P. B Russell, J. M. Livingston, and L. A. Remer. Case studies of aerosol remote sensing in the vicinity of clouds. *J. Geophys. Res.*, 114, 2009. doi: 10.1029/2008JD010774.

L. A. Remer, Y. J. Kaufman, D. Tanré, S. Mattoo, D. A. Chu, J. V. Martins, R.-R. Li, C. Ichoku, R. C. Levy, R. G. Kleidman, T. F. Eck, E. Vermote, and B. N. Holben. The MODIS aerosol algorithm, products, and validation. *J. Atmos. Sci.*, 62(4):947–973, 2005. doi: 10.1175/JAS3385.1.

D. M. Romps and Z. Kuang. Overshooting convection in tropical cyclones. *Geophys. Res. Lett.*, 36: L09804, 2009. doi: 10.1029/2009GL037396.

D. Rosenfeld. Suppression of Rain and Snow by Urban and Industrial Air Pollution. *Science*, 287: 1793–1796, 2000.

D. Rosenfeld and I. M. Lensky. Satellite-Based Insights into Precipitation Formation Processes in Continental and Maritime Convective Clouds. *B. Am. Meteorol. Soc.*, 79(11):2457–2476, 1998.

D. Rosenfeld, U. Lohmann, G. B. Raga, C. D. O'Dowd, M. Kulmala, S. Fuzzi, A. Reissell, and M. O. Andreae. Flood or Drought: How Do Aerosols Affect Precipitation? *Science*, 321(5894): 1309–1313, 2008.

B. M. Sanderson, R. Knutti, T. Aina, C. Christensen, N. Faull, D. J. Frame, W. J. Ingram, C. Piani, D. A. Stainforth, D. A. Stone, and M. R. Allen. Constraints on model response to greenhouse gas forcing and the role of subgrid-scale processes. *J. Climate*, 21(11):2384–2400, 2008a. doi: 10.1175/2008JCLI1869.1.

B. M. Sanderson, C. Piani, W. J. Ingram, D. A. Stone, and M. R. Allen. Towards constraining climate sensitivity by linear analysis of feedback patterns in thousands of perturbed-physics GCM simulations. *Clim. Dynam.*, 30(2–3):175–190, 2008b. doi: 10.1007/s00382-007-0280-7.

A. M. Sayer. *Aerosol Remote Sensing Using AATSR*. PhD thesis, University of Oxford, 243pp., 2008.

C. M. Sheih, S. A. Johnson, and F. T. DePaul. Case studies of aerosol size distribution and chemistry during passages of a cold and a warm front. *Atmos Environ*, 17(7):1299–1306, 1983. ISSN 0004-6981. doi: 10.1016/0004-6981(83)90404-3.

D. T. Shindell. Climate and ozone response to increased stratospheric water vapor. *Geophys. Res. Lett.*, 28(8):1551–1554, 2001. doi: 10.1029/1999GL011197.

D. Stainforth, J. Kettleborough, M. Allen, M. Collins, A. Heaps, and J. Murphy. Distributed computing for public-interest climate modeling research. *Comput. Sci. Eng.*, 4(3):82–89, 2002. doi: 10.1109/5992.998644.

D. A. Stainforth, T. Aina, C. Christensen, M. Collins, N. Faull, D. J. Frame, J. A. Kettleborough, S. Knight, A. Martin, J. M. Murphy, C. Piani, D. Sexton, L. A. Smith, R. A. Spicer, A. J. Thorpe, and M. R. Allen. Uncertainty in predictions of the climate response to rising levels of greenhouse gases. *Nature*, 433(7024):403–406, 2005. doi: 10.1038/nature03301.

G. L. Stephens. Cloud feedbacks in the climate system: A critical review. *J. Climate*, 18(2):237–273, 2005. doi: 10.1175/JCLI-3243.1.

B. Stevens and G. Feingold. Untangling aerosol effects on clouds and precipitation in a buffered system. *Nature*, 461:607–613, 2009. doi: 10.1038/nature08281.

P. Stier, J. H. Seinfeld, S. Kinne, and O. Boucher. Aerosol absorption and radiative forcing. *Atmos. Chem. Phys.*, 7(19):5237–5261, 2007.

D. A. Stone, M. R. Allen, F. Selten, M. Kliphuis, and P. A. Stott. The detection and attribution of climate change using an ensemble of opportunity. *J. Climate*, 20(3):504–516, 2007. doi: 10.1175/JCLI3966.1.

K. Suzuki, T. Nakajima, M. Satoh, H. Tomita, T. Takemura, T. Y. Nakajima, and G. L. Stephens. Global cloud-system-resolving simulation of aerosol effect on warm clouds. *Geophys. Res. Lett.*, 35, 2008. doi: 10.1029/2008GL035449.

C. H. Twohy, J. A. Coakley Jr., and W. R. Tahnk. Effect of changes in relative humidity on aerosol scattering near clouds. *J. Geophys. Res.*, 114:D05205, 2009. doi: 10.1029/2008JD010991.

S. Twomey. The Influence of Pollution on the Shortwave Albedo of Clouds. *J. Atmos. Sci.*, 34: 1149–1152, 1977.

Université Lille 1. ICARE: Cloud-Aerosol-Water-Radiation Interactions, 2009. `http://www.icare.univ-lille1.fr/` [Accessed 22nd August 2009].

University of Oxford. GRAPE: Global Retrieval of ATSR Cloud Parameters and Evaluation, 2009a. `http://www.atm.ox.ac.uk/project/grape/index.html` [Accessed 21st August 2009].

University of Oxford. Oxford-RAL Retrieval of Aerosol and Cloud (ORAC), 2009b. `http://www.atm.ox.ac.uk/project/ORAC/index.html` [Accessed 21st August 2009].

B. Vant-Hull, A. Marshak, L. A. Remer, and Z. Q. Li. The effects of scattering angle and cumulus cloud geometry on satellite retrievals of cloud droplet effective radius. *IEEE T. Geosci. Remote*, 45(4):1039–1045, 2007. doi: 10.1109/TGRS.2006.890416.

C.-C. Wang and J. C. Rogers. A Composite Study of Explosive Cyclogenesis in Different Sectors of the North Atlantic. Part I: Cyclone Structure and Evolution. *Mon. Weather Rev.*, 129:1481–1499, 2001.

F. Waquet, J. Riedi, L. C. Labonnote, P. Goloub, B. Cairns, J.-L. Deuzé, and D. Tanré. Aerosol Remote Sensing over Clouds Using A-Train Observations. *J. Atmos. Sci.*, 66(8):2468–2480, 2009. doi: 10.1175/2009JAS3026.1.

S. G. Warren, R. M. Eastman, and C. J. Hahn. A Survey of Changes in Cloud Cover and Cloud Types over Land from Surface Observations, 1971–96. *J. Climate*, 20:717–738, 2007. doi: 10.1175/JCLI4031.1.

D. M. Winker, W. H. Hunt, and M. J. McGill. Initial performance assessment of CALIOP. *Geophys. Res. Lett.*, 34(19):L19803, 2007. doi: 10.1029/2007GL030135.

R. Wood, C. R. Mecheso, C. S. Bretherton, B. Huebert, and R. Weller. The VAMOS Ocean-Cloud-Atmosphere-Land Study (VOCALS). *U.S. CLIVAR Variations*, 5(1), 2007.

D. L. Wu, S. A. Ackerman, R. Davies, D. J. Diner, M. J. Garay, B. H. Kahn, B. C. Maddux, C. M. Moroney, G. L. Stephens, J. P. Veefkind, and M. A. Vaughan. Vertical distributions and relationships of cloud occurrence frequency as observed by MISR, AIRS, MODIS, OMI, CALIPSO, and CloudSat. *Geophys. Res. Lett.*, 36:L09821, 2009. doi: 10.1029/2009GL037464.